



# $^{10}\text{Be}$ and $^{14}\text{C}$ data provide insight on soil mass redistribution along gentle slopes and reveal ancient human impact

Francesca Calitri<sup>1,2,3</sup> · Michael Sommer<sup>2,3</sup> · W. Marijn van der Meij<sup>2,4</sup> · Dmitry Tikhomirov<sup>1</sup> · Marcus Christl<sup>5</sup> · Markus Egli<sup>1</sup>

Received: 16 March 2021 / Accepted: 27 July 2021 / Published online: 11 August 2021  
© The Author(s) 2021

## Abstract

**Purpose** Spatial and temporal patterns of past erosional events are a useful and needed information to explain observed soil patterns in different landscapes. Soil thickness reflects the overall expression of pedogenesis and erosion. Forested soils of Northern Germany exhibit varying soil thicknesses with thin soils on crest positions and buried soils at the footslope. The aim of this study is to reconstruct the complex soil mass redistribution and soil patterns of this forested area due to different periods of erosion and stability.

**Methods** We explored the explanatory power of both  $^{10}\text{Be}$  (in situ and meteoric) on a hillslope and we  $^{14}\text{C}$ -dated buried horizons at different depths.

**Results** The  $^{10}\text{Be}$  depth profiles did not show an exponential decrease with depth. They had a ‘bulge’ shape indicating clay translocation and interaction with oxyhydroxydes (meteoric  $^{10}\text{Be}$ ), bioturbation and soil mass redistribution (in situ  $^{10}\text{Be}$ ). The combined application of both  $^{10}\text{Be}$  and  $^{14}\text{C}$  dating revealed progressive and regressive phases of soil evolution. Although Melzower Forest is protected (same vegetation) since the past 250 years, both  $^{10}\text{Be}$  clearly indicated major soil mass redistribution along the investigated catena.

**Conclusion** A strong erosion impulse must have occurred between 4.5 and 6.8 kyr BP indicating an earlier human impact on soil erosion than previously postulated (~3 kyr earlier). Our findings correlate in fact with the first settlements reported for this region (~6.8 kyr BP) and show their immediate effect on soils. The overall soil redistribution rates in this forest are surprisingly similar to those obtained from a nearby agricultural area.

**Keywords** Soil redistribution · Erosion ·  $^{10}\text{Be}$  · Forest · Catena

---

Responsible editor: Heike Knicker

✉ Francesca Calitri  
francesca.calitri@geo.uzh.ch

<sup>1</sup> Department of Geography, University of Zurich,  
Winterthurerstrasse 190, 8057 Zurich, Switzerland

<sup>2</sup> Landscape Pedology Working Group, Leibniz-Centre  
for Agricultural Landscape Research (ZALF), Eberswalder  
Straße 84, 15374 Müncheberg, Germany

<sup>3</sup> Institute of Environmental Science and Geography,  
University of Potsdam, Karl-Liebknecht-Str.24-25,  
14476 Potsdam, Germany

<sup>4</sup> Institute of Geography, University of Cologne,  
Albertus-Magnus-Platz, 50923 Cologne, Germany

<sup>5</sup> Laboratory of Ion Beam Physics, ETH Zürich, 8093 Zurich,  
Switzerland

## 1 Introduction

Soils are a dynamic system and are the product of environmental and historical factors (Jenny 1984; Birkeland et al. 2003). Consequently, soil thickness and horizonation at a given time-point in its evolution reflect the overall expression of pedogenesis (progressive evolution) and soil erosion (regressive processes; Sommer et al. 2008).

Soil and landscape heterogeneity is mainly caused by variations of parent material, topography, biota and occurrences of apparently random events (e.g. tree uprooting; Minasny et al. 2015; Samonil et al. 2017). Differences in soil properties cause variations in hydraulic properties, which influence patterns of surface runoff and subsurface flow and, together with the variation in soil properties, lead to spatially varying rates of mass redistribution across the landscape (van

Noordwijk et al. 1997; Van Oost et al. 2007; van der Meij et al. 2018). Humans use soil preferentially based on their assumed and experienced suitability for various purposes (such as pasture, arable land, etc.). This leads to patterns of varied land use and, as a consequence, the formation of heterogeneous landscapes (Minasny et al. 2015).

One of the most important processes shaping the land surface and soil profiles is the lateral transport of soil material by erosion. On agricultural land of mid to high latitudes, water erosion has been assumed to be the dominant mode since pre-historic times, with the first evidence of erosion coinciding with the first settlers (Troeh et al. 1981; Montgomery 2007; Brevik and Hartemink 2010). In fact, many European landscapes have been altered by anthropogenic activities (e.g. land use change, deforestation, etc.) since the Neolithic (Kappler et al. 2018). However, the share of soil erosion by tillage and human influence appeared to be even more important in historical and recent times (Van Oost et al. 2005; Wilken et al. 2020). Erosion continuously moves soil material from upslope to downslope (Heimsath et al. 1997) or even the other way round (caused by tree uprooting; Šamonil et al. 2017). From a geomorphological perspective (black box approach), the soil thicknesses are in steady state, when the lowering rate of the soil–bedrock interface, so-called “soil production”, is equivalent to the surface lowering rate, caused by erosion (Heimsath 2006).

The development of isotopic techniques has facilitated the quantification of long-term geomorphic processes at the Earth’s surface (Banner 2004; Ivy-Ochs and Kober 2008; Preusser et al. 2008). Cosmogenic isotopes that are formed in minerals at the Earth’s surface (in situ) or in the atmosphere (meteoric) are now commonly used for dating and determining physical erosion and denudation rates (Schoonejans et al. 2017). Soil production and denudation rates can be assessed by using meteoric or in situ produced  $^{10}\text{Be}$ . Both deposition and soil erosion can be evaluated from meteoric  $^{10}\text{Be}$  (using inventories similar to fallout radionuclide methods; Maejima et al. 2005; Egli et al. 2010; Hidy et al. 2010). Burial may also be apparent from in situ  $^{10}\text{Be}$  profiles, but so far, in situ  $^{10}\text{Be}$  has only been used for the quantification of denudation and erosion.

The depth variations of in situ  $^{10}\text{Be}$  concentrations within a weathering profile are a powerful approach to constrain geomorphological parameters, including the mean denudation rate (e.g. Siame et al. 2004; Dosseto and Schaller 2016). In geochemical studies, meteoric  $^{10}\text{Be}$  is often used as a tracer for soil thickness development (McKean et al. 1993; Jungers et al. 2009; Willenbring and von Blanckenburg 2010; West et al. 2013) and regolith residence time (e.g. Pavich 1989; Bacon et al. 2012).

With the combination of both types of  $^{10}\text{Be}$ , the dynamics of soils and related mass transports should be even more traceable. We explored the explanatory power of both  $^{10}\text{Be}$

forms in forested soils along a catena in the hummocky ground moraine landscape of northeastern Germany. These soils have been forested for at least 250 years, but exhibit strongly varying thicknesses with very shallow soils on crest positions (Rüffer 2018) and soils up to 1.5 m at the foot-slope, due to (pre-)historical erosion processes (Rüffer 2018; Calitri et al. 2020). The aim of this study is to reconstruct the complex soil mass redistribution and soil patterns of this forested area due to different periods of erosion and stability. We  $^{14}\text{C}$ -dated buried horizons found in five footslope/back-slope positions in the catchment to determine erosion periods and we measured both in situ and meteoric  $^{10}\text{Be}$  distributions along a soil catena to calculate erosion and deposition rates. With these data, we complement a previous study done in the same region on intensively used agricultural soils to understand what  $^{10}\text{Be}$  distributions indicate in terms of soil processes (e.g. erosion, sedimentation) and how and when anthropogenic processes influenced soil mass redistribution and soil patterns (Calitri et al. 2019).

## 2 Study area

The study area is located in the Uckermark region, northeastern Germany, which is a formerly glaciated landscape (Fig. 1). The area has a hummocky terrain characterised by knolls, a series of small lakes and kettle holes (Calitri et al. 2019). The kettle holes are closed catchments, which allow quantification of soil erosion and deposition rates by mass balance calculations. The hummocky ground moraine shows a pronounced small-scale variation of soil properties and soil units as a function of topography (Koszinski et al. 2013; van der Meij et al. 2017).

The study region is characterised by a subcontinental climate with a mean annual temperature of 8.9 °C and mean annual precipitation of about 500 mm (Kopp and Schwanecke 1994). The climatic water balance is slightly negative (with about  $-25 \text{ mm year}^{-1}$ ). We selected the “Melzower Forst” as study area in the region (Calitri et al. 2020). The Melzower Forst is an old forest complex, which has been forested for at least the last 250 years, according to historical maps of the late eighteenth century. It consists of an old beech tree forest (*Fagus sylvatica* L.) with some individuals having an age of up to 400 years (Rüffer 2018).

We selected the study area “Melzower Forst” to compare it with an intensively studied agricultural site on hummocky ground moraines (“CarboZALF-D,” Calitri et al. 2019). These sites share similar soil forming factors (e.g. climate, terrain, parent material), except for land use (Calitri et al. 2020). Through this comparison, we want to assess the effect of land use on erosion rates.

The parent material for soil development is an illitic, calcareous glacial till. According to the geological map

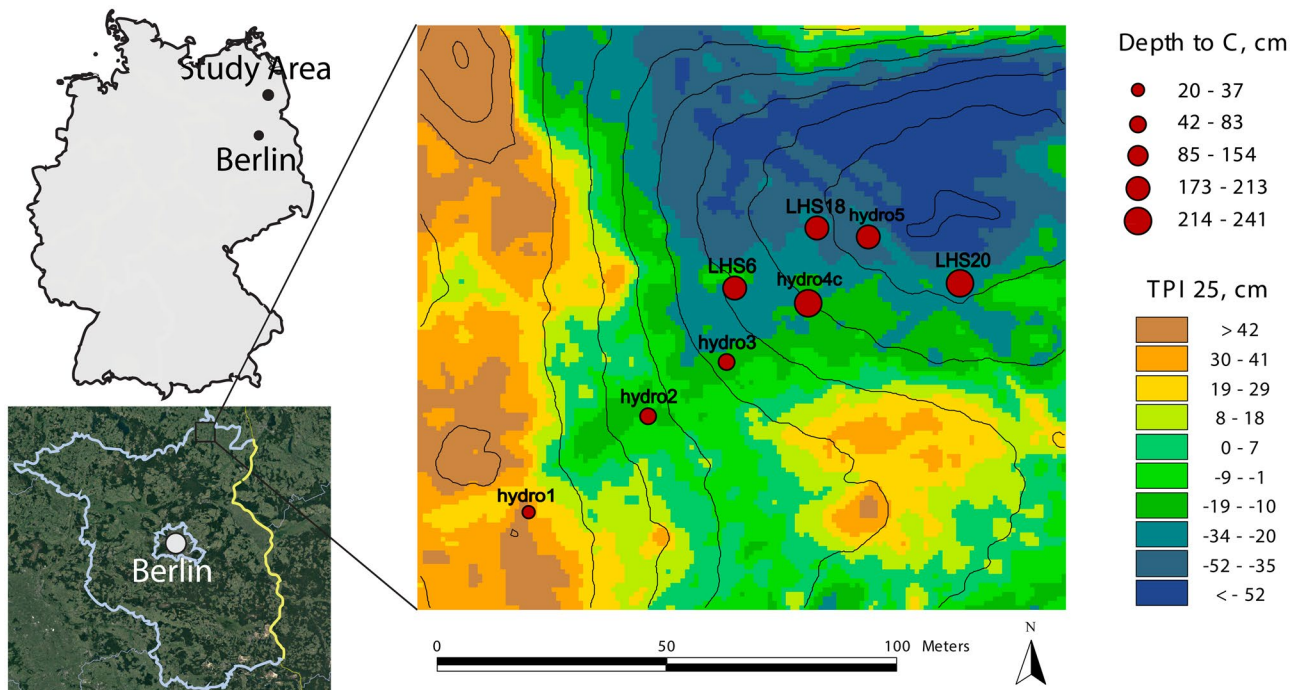


**Fig. 1** Map of Germany and the study area ‘Melzower Forst’ (left). Relationship between terrain parameters and soil thickness (depth to C horizons) and spatial pattern of the TPI (Topographic Position Index; right)

of Brandenburg (<http://www.geo.brandenburg.de/boden/>; Geologische Übersichtskarte, Dezernat Geologische Landesaufnahme/Geoarchiv), the morainic deposits are from the Pleistocene, have a granitic character (Si-rich), are marly and also contain some carbonates. Loess does not occur in this region, because it was fully glaciated (Calitri et al. 2019). These forest soils exhibit strongly varying thicknesses with very shallow soils, Calcaric Regosols (FAO 2006; IUSS Working Group WRB 2015), on crest positions (Rüffer 2018) and soils up to 1.5 m at the footslope (Stagnic Albic Retisols, IUSS Working Group WRB 2015) (Calitri et al. 2020).

### 3 Materials and methods

#### 3.1 Sampling strategy

A first soil survey at the “Melzower Forst” was completed in November 2016 and consisted of a total of 29 soil corings down to a maximum depth of 3 m. The sampling scheme was designed to select a variety of topographic positions through a conditioned Latin hypercube sampling design ( $n=20$ , Minasny and McBratney 2006), with additional points along a flow path (“hydrosequence”,  $n=5$ ) and on selected locations based on expert knowledge to cover the full soils’ feature space ( $n=4$ ). For the sampling,

we used polypropylene (PP) tubes with a diameter of 63 mm (HT DN63) and a length of 2 + 1 m. Each PP tube was inserted in a closed, metal driving core tube (M22; Nordmeyer Geotool, Herne, Germany) that was driven into the soil by a self-propelled vehicle (GTR 790; Nordmeyer Geotool).

From the 29 coring sites, 16 sites were selected to assess recent soil erosion/deposition rates using plutonium (Pu) inventories (Calitri et al. 2020) and three to assess soil redistribution rates along a catena using  $^{10}\text{Be}$  (this study). We analysed both types of  $^{10}\text{Be}$ : in situ produced and meteoric  $^{10}\text{Be}$  in the soils. For this purpose, a second sampling campaign was carried out in November 2017. At the three sites along the catena (Hydro1, crest position; Hydro 3, backslope position; Hydro4c, footslope position; Fig. 2), we sampled three soil cores down to the parent material (Hydro1 and Hydro3, 45 and 200 cm respectively) and down to a buried horizon (c. 175 cm; Hydro4c). To obtain enough material for in situ  $^{10}\text{Be}$  analyses, we combined samples per horizon and depth: around 5–6 kg of soil material was necessary to attain enough quartz (extracted from the 0.25–0.50-mm fraction; see below). From these samples, an aliquot of a few hundred grams was taken to perform analyses for meteoric  $^{10}\text{Be}$ .

For radiocarbon dating of fossil Ah horizons, we selected other 4 sites from the first sampling campaign (Hydro5, LHS6, LHS18, LHS20 in Fig. 1).

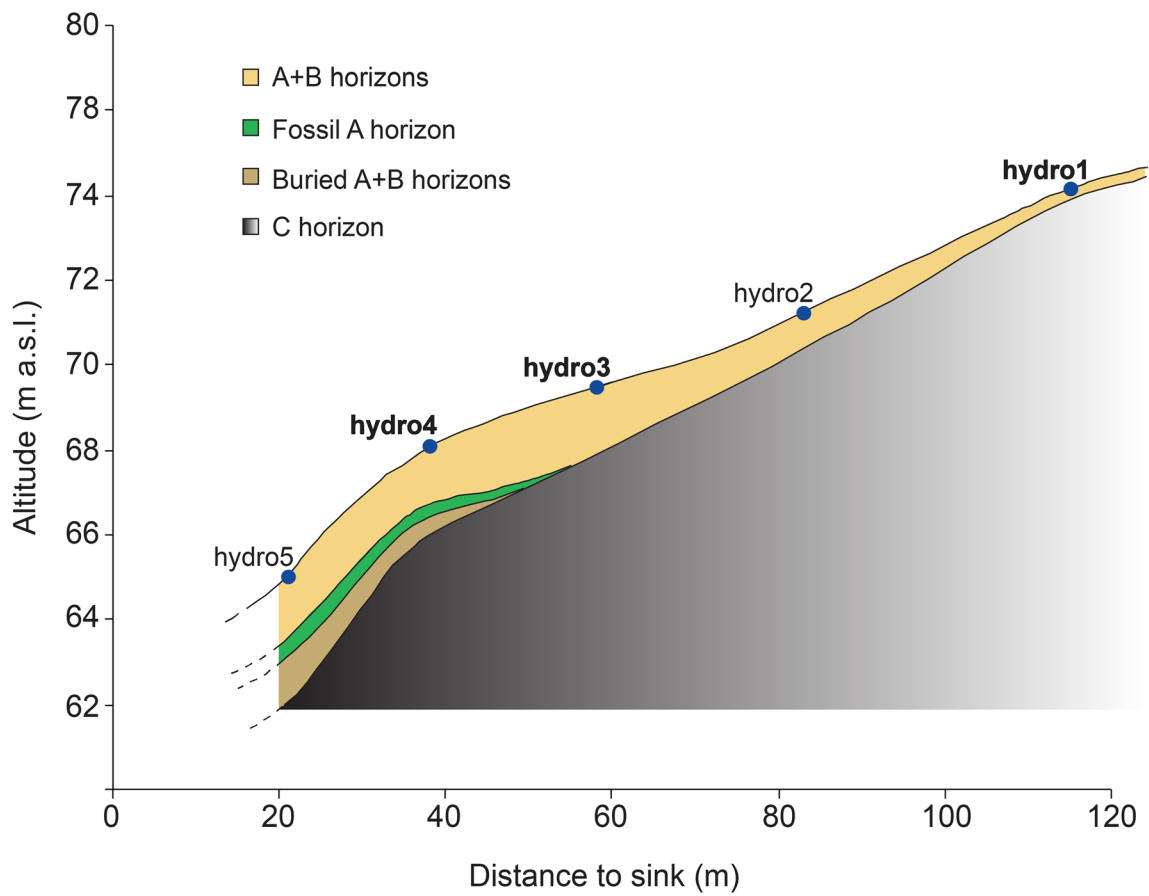
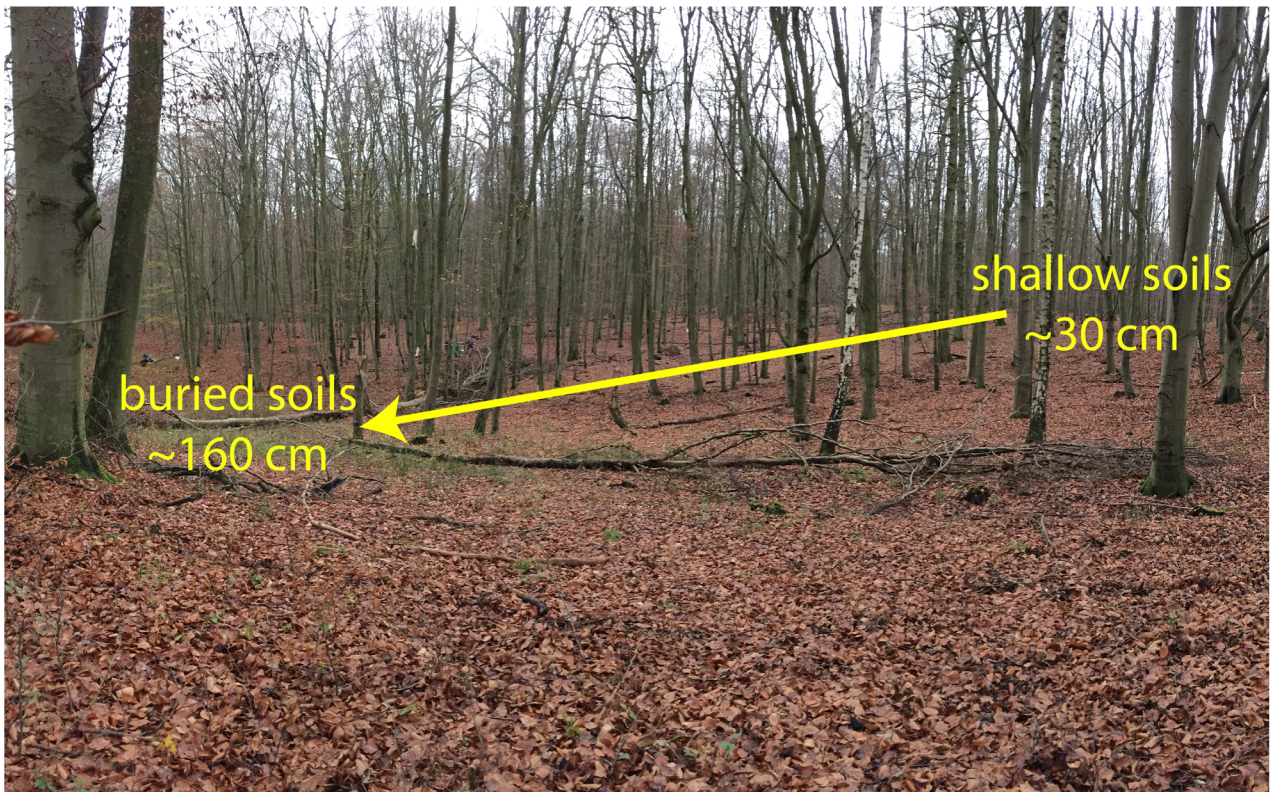


**Fig. 2** Picture of Melzower Forst and schematic cross section (using a vertical exaggeration of a factor 3) of the investigated catena (hydro-sequence with sites Hydro1, Hydro2, Hydro3, Hydro4c, Hydro5)

### 3.2 Soil chemical and physical analyses

Soil samples from cores were dried at 60 °C in the oven, gently crushed and separated with a 2-mm sieve (fine earth < 2 mm; gravel > 2 mm). To determine the particle size distribution of the fine earth fraction, a combination of wet sieving (> 63 µm) and pipette (< 20 µm) method (Schlichting et al. 1995) was used. Particle size analysis pre-treatment consisted of three steps: (i) oxidation of organic matter using H<sub>2</sub>O<sub>2</sub> (10 Vol.%) at 80 °C, (ii) carbonate dissolution with 0.5 N HCl (80 °C) and (iii) dispersion by mixing for 16 h with a 0.01-M Na<sub>4</sub>P<sub>2</sub>O<sub>7</sub> solution (Schlichting et al. 1995). Soil pH was measured using a glass electrode in 0.01-M CaCl<sub>2</sub> suspensions with a soil:solution ratio of 1:2.5 (w/v) after a 60-min equilibration period (Schlichting et al. 1995). Samples were combusted in an elemental analyser (Vario EL, Elementar Analysensysteme, Hanau, Germany) to measure total carbon and nitrogen contents. Carbonate (CaCO<sub>3</sub>) was determined by electrolytic conductivity using the Scheibler apparatus (Schlichting et al. 1995). Organic carbon (C<sub>org</sub>) was calculated as the difference between total carbon and inorganic carbon. All the analyses of the soil properties listed above were performed in two lab replicates per sample.

Total elemental contents were determined using X-ray fluorescence (XRF). Finely milled samples of approximately 5 g were analysed using an energy-dispersive He-flushed X-ray fluorescence spectrometer (ED-XRF, SPECTRO X-LAB 2000, SPECTRO Analytical Instruments, Germany). The quality of the analyses was checked using a soil reference material with certified total element concentrations (Reference Soil Sample CCRMP SO-4, Canada Centre for Mineral and Energy Technology).

### 3.3 Radiocarbon dating of organic matter fractions

The site Hydro 4c and four other soil profiles (Table 5; Fig. 1) have an older buried soil beneath a more recent soil. To date accumulation, soil organic matter of the buried soil was radiocarbon dated. Soil organic carbon contains several fractions: labile fractions with faster turnover along with more stable fractions having an older radiocarbon age (Eusterhues et al. 2005; Helfrich et al. 2007; Kögel-Knabner et al. 2008; Favilli et al. 2009). Particulate organic matter (POM) was dated to approximately date the burial of the fossil soil at these sites. This organic fraction usually contains the youngest organic compounds and is thus a good indicator of the burial event (Favilli et al. 2009). Furthermore, we dated the H<sub>2</sub>O<sub>2</sub>-resistant fraction. This approximately

indicates the oldest organic matter and gives an indication about the start of soil development (Favilli et al. 2009). The extraction of the organic matter fractions was done as described in Favilli et al. (2008).

The carbon ratios were measured by accelerator mass spectrometry (AMS) using the 0.2-MV radiocarbon dating facility (MICADAS) of the Ion Beam Physics at the Swiss Federal Institute of Technology Zurich (ETHZ). The calendar ages were obtained using the OxCal 4.4 calibration program (Bronk Ramsey 2001, 2009) based on the IntCal 20 calibration curve (Reimer et al. 2020). Calibrated ages are reported with their 2σ error range.

### 3.4 Sample preparation and measurement for <sup>10</sup>Be analyses

Sample preparation for meteoric and in situ <sup>10</sup>Be is described in detail in Calitri et al. (2019). In brief: to extract meteoric <sup>10</sup>Be, 2 g of soil sample was milled to a fine powder that was spiked with 1 mg of the commercial <sup>9</sup>Be carrier (Flucka 14205) and leached in HCl (16%). Be was extracted from the leachate in the two consecutive steps: hydroxide co-precipitation and chromatographic separation on Bio-Rad AG50-X8 resin.

To obtain in situ <sup>10</sup>Be, 30 g of pure quartz was separated from the rest of the soil sample (fraction of 250–500 µm) by froth flotation and leached in an HF solution. The quartz was spiked with 0.35 mg of the commercial <sup>9</sup>Be carrier (Scharlau BE3460100) and dissolved in concentrated HF. The resulting fluorides were converted into chlorides and went through a chromatographic separation on Bio-Rad AG1-X8 and AG50-X8 resins.

The purified samples (meteoric and in situ <sup>10</sup>Be) were then precipitated into a hydroxide form, calcinated and mixed with niobium powder prior to accelerator mass spectrometry (AMS) measurement. <sup>10</sup>Be/<sup>9</sup>Be ratios were measured with the TANDY AMS system at the Laboratory of Ion Beam Physics, ETH Zurich (Christl et al. 2013). The measured ratios were normalised to the ETH Zurich in-house secondary standards S2007N and/or S2010N.

### 3.5 Calculation of mass redistribution rates

We applied different methods to calculate soil redistribution rates, using both meteoric and in situ <sup>10</sup>Be contents.

#### 3.5.1 Long-term redistribution rates using meteoric <sup>10</sup>Be

Soils build up <sup>10</sup>Be in time by atmospheric deposition (meteoric <sup>10</sup>Be). The theoretical abundance of <sup>10</sup>Be for a particular site can be calculated by knowing the soil age of that landform by independent dating. Measuring the meteoric <sup>10</sup>Be concentrations in the soil allows the estimation of soil redistribution

rates (Maejima et al. 2005; Egli et al. 2010). Consequently, soil erosion and deposition can be calculated by comparing the measured <sup>10</sup>Be concentrations with the theoretical concentrations for the expected age. The surface age of the investigated site was estimated to be 19 to 20 ka based on the timing of deglaciation (Lüthgens et al. 2011; Hughes et al. 2016; Stroeven et al. 2016). Considering no erosion, the surface age of a soil is given by

$$t = -\frac{1}{\lambda} \ln \left( 1 - \lambda \frac{N_{exp}}{q} \right) \tag{1}$$

and

$$N_{exp} = q \frac{e^{-\lambda t} - 1}{-\lambda} \tag{2}$$

where  $N_{exp}$  (atoms cm<sup>-2</sup>) = calculated theoretical <sup>10</sup>Be inventory in the profile based on the soil age assuming no erosion,  $q$  (atoms cm<sup>-2</sup> year<sup>-1</sup>) = annual <sup>10</sup>Be deposition rate (calculated according to Masarik and Beer 2009; Willenbring and von Blanckenburg 2010),  $\lambda$  (4.997 × 10<sup>-7</sup> a<sup>-1</sup>) = decay constant of <sup>10</sup>Be and  $t$  (a) = soil age. As stated by Egli et al. (2010), <sup>10</sup>Be deposition rates need to be estimated for a specific area. We estimated a deposition rate of ~ 10<sup>6</sup> atoms cm<sup>-2</sup> year<sup>-1</sup> (Masarik and Beer 2009) for the study area, taking into account the geomagnetic latitude. Considering soil erosion, Eq. 1 is broadened to a non-steady-state approach (Zollinger et al. 2017):

$$t = -\frac{1}{\lambda} \ln \left( 1 - \lambda \frac{N}{q - \rho C_{10Be} f E_{soil}} \right) \tag{3}$$

and

$$E_{soil} = \frac{1}{\rho f C_{10Be}} \left( \frac{\lambda N}{e^{-\lambda t} - 1} + q \right) \tag{4}$$

where  $C_{10Be}$  (atoms g<sup>-1</sup>) = average <sup>10</sup>Be content in the top eroding soil,  $E_{soil}$  = soil erosion rate (cm year<sup>-1</sup>),  $f$  = fine earth fraction and  $\rho$  (g cm<sup>-3</sup>) = bulk density of the topsoil. Due to the evolution over time of  $C_{10Be}$ , we use an average value between  $t = 0$  and  $t$  of ~ 0.5 ×  $C_{10Be(today)}$  and assume that erosion losses are concentrated on the topsoil (e.g. 0–20 cm). We obtain

$$\frac{N_{exp} - N}{t} = \frac{\Delta N}{t} = E(N) \tag{5}$$

where  $E(N)$  (atoms cm<sup>-2</sup> year<sup>-1</sup>) = annually eroded <sup>10</sup>Be. As a result, the annual erosion rate ( $E_{soil}$ ; cm year<sup>-1</sup>) is resulting in

$$E_{soil} = \frac{z_{top} E(N)}{N_{top}} \tag{6}$$

where  $N_{top}$  = <sup>10</sup>Be content in the topsoil (with the thickness  $z_{top}$ ). To convert erosion rates to tons per square kilometre per year,  $E_{soil}$  has to be multiplied by soil density and referred to square kilometres. The concentrations of <sup>10</sup>Be measured in the C-horizon are used to calculate the <sup>10</sup>Be content due to pre-exposure.

An additional procedure (Lal 2001) was applied to estimate erosion rates using meteoric <sup>10</sup>Be and compare the different methods. The soil erosion ( $E_{soil}$ ) rate is calculated as

$$E_{soil} = z_0 K_E \tag{7}$$

and

$$K_E = \frac{N_D}{N_S} \left[ \frac{Q + q_a}{N_D} - \lambda \right] - \lambda \tag{8}$$

where  $z_0$  (cm) = thickness of topsoil horizons (consist of O and A horizons),  $K_E$  = first-order rate constant for removal of soil from the topsoil layer,  $N_S$  (atoms cm<sup>-2</sup>) = <sup>10</sup>Be inventory in topsoil horizons,  $N_D$  (atoms cm<sup>-2</sup>) = <sup>10</sup>Be inventory in the D layer (usually consists of B and C horizons or the rest of the soil profile),  $Q$  (atoms cm<sup>-2</sup> year<sup>-1</sup>) = flux of meteoric <sup>10</sup>Be into the topsoil and  $q_a$  (atoms cm<sup>-2</sup> year<sup>-1</sup>) = flux of meteoric <sup>10</sup>Be.

These approaches were suitable only for the sites Hydro1 and Hydro3 as a result of their meteoric <sup>10</sup>Be depth trends.

### 3.5.2 Long-term redistribution rates using in situ <sup>10</sup>Be

Hidy et al. (2010) developed a depth profile model for sediments that are not vertically mixed to estimate changes in the in situ terrestrial cosmogenic nuclide production rate considering that secondary cosmic ray flux attenuates through materials. In this case study, the following model was applied to the sites Hydro1 and Hydro3.

The concentration  $C$  (atoms g<sup>-1</sup>) for a specific nuclide  $m$  that is produced only from high-energy nuclear and muogenic reactions (e.g. <sup>10</sup>Be, <sup>14</sup>C, <sup>26</sup>Al, <sup>21</sup>Ne) and is a function of depth  $z$  (cm), erosion rate  $\epsilon$  (cm year<sup>-1</sup>) and exposure time  $t$  can be defined as

$$C_m(z, \epsilon, t) = \sum_i \frac{P(0)_{m,i}}{\left( \frac{\epsilon \rho_z}{\Lambda_i} + \lambda_m \right)} \cdot \exp \left( -\frac{z \rho_z}{\Lambda_i} \right) \cdot \left[ 1 - \exp \left( -t \left( \frac{\epsilon \rho_z}{\Lambda_i} + \lambda_m \right) \right) \right] + C_{inh,m} \cdot \exp(-\lambda_m t) \tag{9}$$

where  $i$  stands for the different production pathways for nuclide  $m$  (neutron spallation, fast muon spallation, and negative muon capture),  $P(0)_{m,i}$  is the site-specific surface production rate for nuclide  $m$  via production pathway  $i$  (in this case,  $4.29 \text{ atoms g}^{-1} \text{ year}^{-1}$ ),  $\lambda_m$  is the decay constant for nuclide  $m$  ( $\text{a}^{-1}$ ),  $\rho_z$  is the cumulative bulk density at depth  $z$  ( $\text{g cm}^{-3}$ ),  $\Lambda_i$  is the attenuation length of production pathway  $i$  ( $160 \text{ g cm}^{-2}$  for neutrons) and  $C_{inh,m}$  is the inherited (depositional) concentration of nuclide  $m$  ( $\text{atom g}^{-1}$ ). The depth trends were modelled using Eq. (9) and a Monte Carlo simulation. Each individual, the modelled depth trend of the  $^{10}\text{Be}$  content was compared to the observed values and iteratively fitted (using erosion rates and inherited  $^{10}\text{Be}$ ) until the differences were minimal. In case of vertical mixing, i.e. clay translocation of the depth profile, as observed in our study area, modelling becomes more difficult. Nonetheless, with sufficient data points, the trend can equally be traced.

In the case of well-mixed soils,  $^{10}\text{Be}$  can still be used to determine erosion rates at the landscape scale from stream sediments and at the plot scale for soil production rates (i.e. Granger and Riebe 2007, 2014; Norton et al. 2010). For this purpose, we used the ‘CRONUS’ online calculator for erosion rate estimate (Balco et al. 2008; <http://hess.ess.washington.edu/>). Erosion rates were calculated using an average  $^{10}\text{Be}$  concentration of the top ~60 cm, assuming that these represent an average surface content due to the complete mixing.

### 3.6 Data and statistical analyses

Linear, multiple linear and polynomial (second order) regressions were carried out to help explain the behaviour of  $^{10}\text{Be}$  in the soils and describe it as a function of controlling factors. All data that were considered for this analysis showed a normal distribution (Shapiro–Wilk test).

## 4 Results

### 4.1 Morphological, physical and chemical soil properties

The soil thicknesses as derived from the depth to C-horizons increase along the catena (Tables 1 and 2; Fig. 1; see also

Calitri et al. 2020). The intensity of redoximorphism increases towards the lower slope soils but is mostly restricted to subsoil horizons (see horizon designations in Table 2). All studied soils have a sandy-loamy to loamy texture and a low gravel content except for a few horizons at the Hydro3 site (Table 2). Clay translocation from eluvial to illuvial soil horizons is clearly recognisable as the main pedogenic process along the catena (Fig. 3). Hydro1 classifies as a Nudiargic Luvisol, Hydro3 as an Endostagnic Albic Retisol and Hydro4c as a Katostagnic Albic Retisol (IUSS Working Group WRB 2015; Table 1). The clay increase towards the illuvial horizons (Bt) in Hydro3 is almost twice as high as in Hydro4c. Together with the much larger total thickness of Bt horizons (Hydro3 83 cm, Hydro4c 30 cm, Table 2), this indicates Hydro3 being exposed to a much longer period of progressive soil development (*ceteris paribus*). The topsoil of Hydro4c is acidic with pH ranging between 3.6 and 5.1. Hydro1 and Hydro3 have pH values ranging from strongly acidic (4.0) to neutral (7.0). The C horizons of Hydro1 and Hydro3 are characterised by higher pH values (7.5) due to carbonates (10%  $\text{CaCO}_3$ ). The soil organic carbon content (SOC) in the Ah horizon ranged from 1.6 to 2.8%.

### 4.2 $^{14}\text{C}$ dating

We analysed soil samples from 5 buried horizons for  $^{14}\text{C}$  dating (Fig. 1; Table 5). The buried horizons are located at similar depths (ca. 180–210 cm) except for the fAh horizon at the LHS6 site (85–108 cm). All calibrated ages (POM fraction) are comparable with an age (1-sigma range) spanning from 4607 to 4448 year cal BP (LHS18) to 6845–6745 year cal BP (Hydro4c). Despite being the most superficially buried horizon (85–108 cm), the fAh horizon at LHS6 is not the youngest (5576–5335 year cal BP).

Three fossil Ah horizons (Hydro5, LHS18, LHS20) treated with hydrogen peroxide ( $\text{H}_2\text{O}_2$ ) treatment showed all comparable ages around 11 kyr cal BP. LHS6 has a slightly younger age 9696–9025 yr cal BP. In contrast, Hydro4c is older than the rest of the soil profiles having an age of 17,560–16,161 year cal BP. The uncertainty in the  $^{14}\text{C}$  measurements of the  $\text{H}_2\text{O}_2$ -treated fraction is relatively high for

**Table 1** Location, landscape attributes and soil characteristics for study site “Melzower Forst”

Site name	Coordinates ( $^{\circ}\text{N}/^{\circ}\text{E}$ )	Slope ( $^{\circ}$ )	TPI25 (m)	dts (m)	Soil classification (IUSS Working Group WRB 2015)	Depth to C (cm)	Fossil Ah, upper boundary (cm)
hydro1	53.152938/13.883513	4.2	0.79	115	Nudiargic Luvisol (LV-ng)	30	-
hydro3	53.153241/13.884138	4.4	-0.23	58	Endostagnic Albic Retisol (RT-stn.ab)	154	-
hydro4c	53.153446/13.884194	4.1	-0.31	38	Katostagnic Albic Retisol (RT-stk.ab)	214	170

dts distance to sink

**Table 2** Physical and chemical characteristics of the investigated soils

Site	Soil type depth (cm)	Soil horizon	>2 mm (%)	Sand (%)	Silt (%)	Clay (%)	Bulk density (Mg/m <sup>3</sup> )	pH (CaCl <sub>2</sub> )	SOC (%)	CaCO <sub>3</sub> (%)	Fe <sub>ox</sub> (g kg <sup>-1</sup> )	Fe <sub>dth</sub> (g kg <sup>-1</sup> )	Al <sub>ox</sub> (g kg <sup>-1</sup> )	Mn <sub>dth</sub> (mg kg <sup>-1</sup> )	
Hydro1 Nudiargic Luvisol	0–15	Ah	2	64	21	15	1.32	6.55	2.08	-	0.9	3.5	0.43	242	
	15–30	Bt	3	60	22	18	1.50	6.97	0.69	0.2	1.0	5.5	0.53	216	
	30–45	Ck	3	56	30	14	1.61	7.61	0.46	10.8	0.7	5.2	0.35	140	
	Hydro3 Endostagnic Albic Retisol	0–15	Ah	5	69	21	10	1.18	4.01	1.59	-	1.6	2.5	0.50	152
		15–30	AE	2	71	21	8	1.35	4.64	0.70	-	1.5	2.5	0.51	271
		30–45	EA	3	73	22	5	1.44	4.94	0.37	-	1.4	2.6	0.45	363
		45–60	E	9	69	21	10	1.45	5.41	0.28	-	1.8	4.0	0.35	306
		60–75	E/Bht	3	66	22	12	1.49	5.59	0.32	-	2.8	5.7	0.43	251
		75–90	Bthg1	2	61	25	14	1.65	5.67	0.31	-	2.6	5.4	0.46	217
		90–105	Bthg2	5	55	28	17	1.63	5.67	0.31	-	2.7	5.7	0.52	157
105–120		Btg1	26	50	26	24	1.68	5.84	0.22	-	2.4	6.5	0.54	160	
120–135		Btg2	6	52	25	23	1.69	6.03	0.23	-	2.3	7.4	0.49	236	
135–158		Btg3	17	49	29	22	1.64	6.81	0.23	-	2.0	8.7	0.48	256	
158–165	Ckg	9	51	35	14	1.78	7.24	0.09	3.2	1.3	8.3	0.36	270		
165–185	Ck	2	52	36	12	1.73	7.50	0.02	9.0	0.6	4.4	0.28	153		
Hydro4c Katostagnic Albic Retisol	0–10	Ah	3	69	23	8	0.71	3.64	2.80	-	1.3	2.9	0.43	159	
	10–20	AE	2	71	22	7	1.13	3.59	1.15	-	1.1	2.7	0.46	121	
	20–29	EA	2	73	21	6	1.22	3.71	0.90	-	1.0	2.4	0.50	168	
	29–40	E	3	69	25	6	1.45	3.96	0.48	-	0.9	2.3	0.49	195	
	40–50	Eg1	3	68	24	8	1.55	4.28	0.21	-	0.8	2.8	0.43	278	
	50–60	Eg2	3	66	24	10	1.60	4.64	0.20	-	0.8	4.0	0.40	299	
	60–70	Eg3	3	64	24	12	1.65	4.89	0.22	-	0.9	4.7	0.42	302	
	70–80	Btg1	3	64	22	14	1.73	4.93	0.22	-	1.0	5.3	0.43	307	
	80–90	Btg2	4	62	23	15	1.69	4.78	0.23	-	1.1	5.7	0.46	337	
	90–100	Btg3	3	63	22	15	1.70	4.71	0.24	-	1.2	5.3	0.45	317	
	100–110	Bg1	6	65	23	12	1.75	4.72	0.23	-	1.3	5.6	0.45	321	
	110–120	Bg2	4	65	24	11	1.79	4.81	0.25	-	1.3	5.4	0.42	338	
	120–130	Bg3	5	67	22	11	1.79	4.88	0.27	-	1.3	4.9	0.40	354	
	130–140	Bg4	3	66	23	11	1.80	4.95	0.21	-	1.3	4.8	0.35	354	
	140–150	Bg5	3	67	22	11	1.80	5.15	0.21	-	1.4	4.8	0.34	351	
	150–158	Bg6	1	65	23	12	1.74	5.15	0.32	-	1.3	5.2	0.38	378	
	158–170	Ab/Bg	2	65	24	11	1.74	5.14	0.47	-	1.4	5.0	0.43	383	
170–175	fAh	1	61	26	13	1.75	5.14	0.69	-	1.5	5.6	0.50	418		



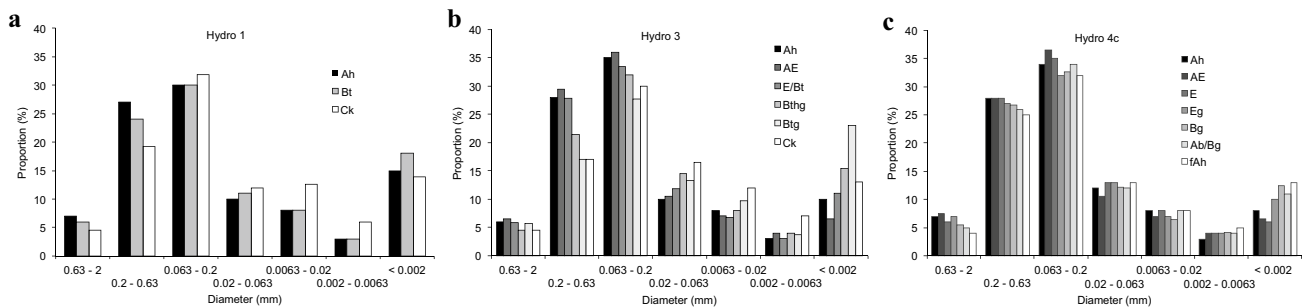


**Fig. 3** Detailed overview of grain sizes as a function of soil horizons for the sites **a)** Hydro1, **b)** Hydro3 and **c)** Hydro4c

all the samples — except for the Hydro4c site — due to a too low amount of material for the AMS measurements. The  $^{14}\text{C}$  ages of the  $\text{H}_2\text{O}_2$ -resistant fraction indicates a start of soil development around 17 kyr BP whereas the  $^{14}\text{C}$  ages of the POM fraction evidence erosional events between about 4.5 and 6.8 kyr BP.

### 4.3 Meteoric and in situ $^{10}\text{Be}$

The contents of meteoric  $^{10}\text{Be}$  as a function of soil depth are given in Fig. 4. The original data are found in the supplementary Table S1. Site Hydro1 has a much lower  $^{10}\text{Be}$  content than Hydro3 or Hydro4c. The highest content was usually found in the subsoil (E/Bth-Hydro3). The  $^{10}\text{Be}$  contents in Hydro1 match with the profile morphology (Ah, thin Bt and C horizon), which suggests that former E and most of the Bt horizons were removed.

Similar to the meteoric  $^{10}\text{Be}$ , the highest content of in situ  $^{10}\text{Be}$  was detected in the EA horizon in the Hydro3 profile (Fig. 4). As in situ  $^{10}\text{Be}$  is measured in quartz, it seems unlikely that the  $^{10}\text{Be}$  profile primarily reflects clay translocation (eluviation/illuviation). This distribution might also be a result of bioturbation, as intense earthworm and mice activity was observed while sampling.

The profile Hydro4c shows an increase in the meteoric  $^{10}\text{Be}$  content with depth and the peak right in the fAh horizon. This might be due to (i) the burial event per se, with the deposition of soil material on the top of an older topsoil and (ii) clay-mediated transport of  $^{10}\text{Be}$  (see Sec. 5.2).

Moreover, we compared the  $^{10}\text{Be}$  contents of the Melzower Forst (Hydro1, Hydro3, Hydro4c) with  $^{10}\text{Be}$  data from an agricultural landscape in a similar geographical setting, the CarboZALF site (with the profiles LP4, LP12N, VAMOS; Fig. 4; Table 1; Calitri et al. 2019). As shown in Fig. 4, the meteoric  $^{10}\text{Be}$  depth profiles of the Melzower Forst are moderately comparable to those at the CarboZALF study site. Both non-eroded soils show similar clay depth functions and comparable depth profiles for both meteoric

and in situ  $^{10}\text{Be}$  (Hydro3, backslope position vs. LP4, plateau position). The two eroded soils with remnants of the former Bt (Hydro 1, LP12N) resemble each other in Be depth functions as well.

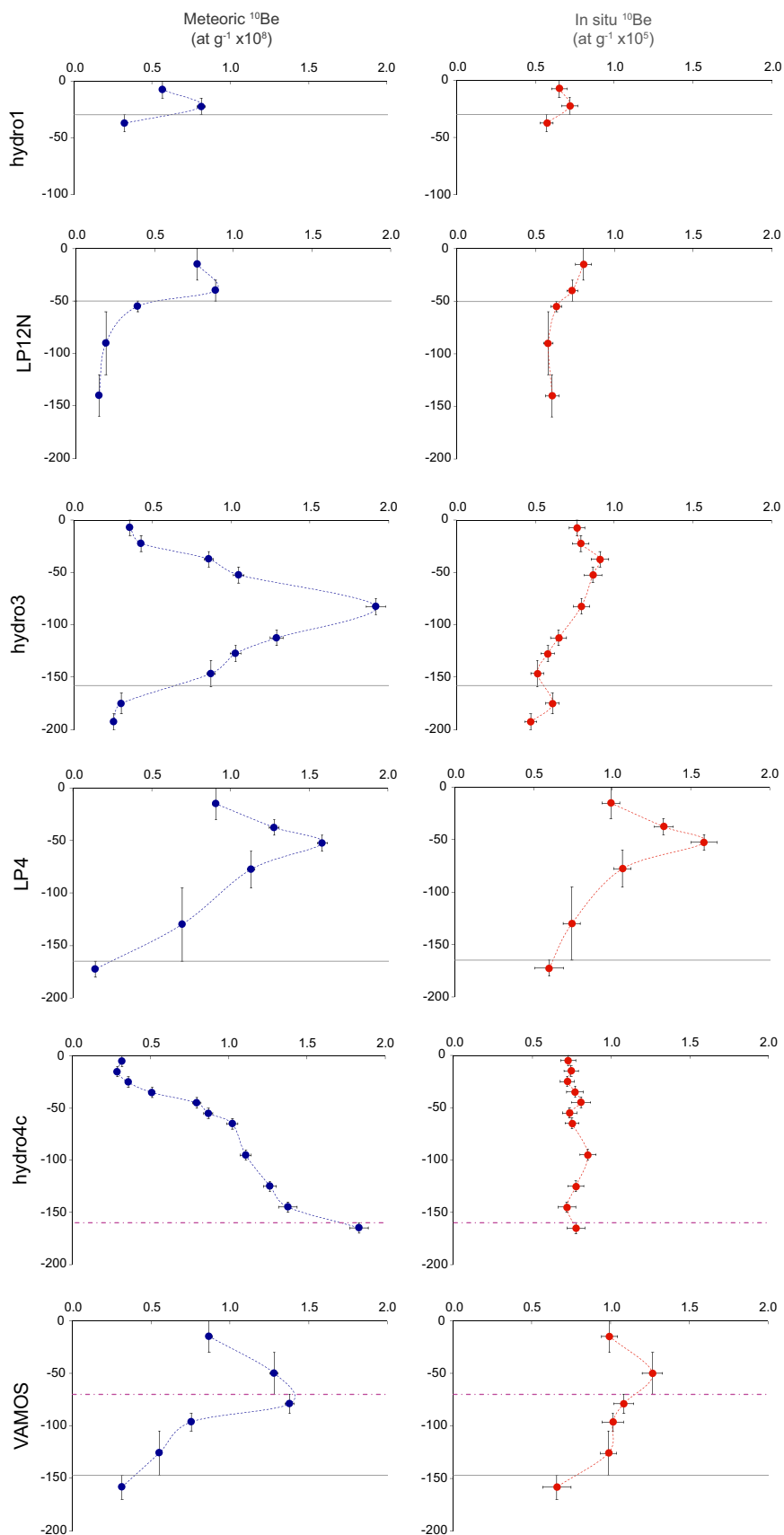
Table 4 shows the relationships between meteoric, in situ  $^{10}\text{Be}$  and physical and chemical properties.  $^{10}\text{Be}$  and pH exhibit the highest correlation. Although the pattern of clay particles along the soil profile and meteoric  $^{10}\text{Be}$  look similar, the correlation between them is not significant.

We found a good correlation of both types of  $^{10}\text{Be}$  with pH (Table 4). In the case of meteoric  $^{10}\text{Be}$ , the correlation has a convex shape with a peak concentration at pH 5.5. Both  $^{10}\text{Be}$  showed a statistically significant correlation with pH,  $\text{Fe}_{\text{dith}}$  and  $\text{Al}_{\text{ox}}$  — meteoric  $^{10}\text{Be}$ :  $R^2 = 0.40$ ,  $p\text{-value} = 0.01$ , in situ  $^{10}\text{Be}$   $R^2 = 0.43$ ,  $p\text{-value} = 0.004$ . Because in situ  $^{10}\text{Be}$  is extracted from quartz of the fraction (250–500  $\mu\text{m}$ ), the relation to pH and pedogenic oxyhydroxides results from similar depth gradients of drivers rather than being causal. Furthermore, Be shows affinities to the major cations Al, Si and Mn, and the lithogenic trace elements neodymium (Nd) and zirconium (Zr) (Ryan 2002). However, in terms of atomic structure and valence state, it is associated with alkaline earth elements. A multilinear regression highlighted a weak correlation between meteoric  $^{10}\text{Be}$  and Nd and Zr ( $R^2 = 0.34$ ;  $p\text{-value} = 0.01$ ; data not shown) for the Melzower Forst.

### 4.4 Soil redistribution rates

The depth function model (Fig. 5) of Hidy et al. (2010) was used to simulate the in situ  $^{10}\text{Be}$  contents along the soil profile and to derive soil erosion rates. This model could be applied successfully to Hydro3 and much less convincingly to profile Hydro1, which had only three data points along the profile. The Hydro4c site exhibited constant in situ  $^{10}\text{Be}$  content along the profile; therefore, modelling was not possible.

**Fig. 4** Depth trends of meteoric  $^{10}\text{Be}$  (at  $\text{g}^{-1}$  fine earth  $< 2 \text{ mm}$   $\times 10^8$ ) and in situ  $^{10}\text{Be}$  (at  $\text{g}^{-1}$  quartz  $250\text{--}500 \mu\text{m}$   $\times 10^5$ ) contents of the forest sites (Melzower Forst) Hydro1 (summit), Hydro3 (backslope) and Hydro4c (footslope) in comparison with depth trends of meteoric and in situ  $^{10}\text{Be}$  of soils in agriculture land (CarboZALF) with the sites LP4, LP12 and VAMOS (Calitri et al. 2019). The grey line represents the C horizon, and the dashed magenta line stands for the fossil A horizon



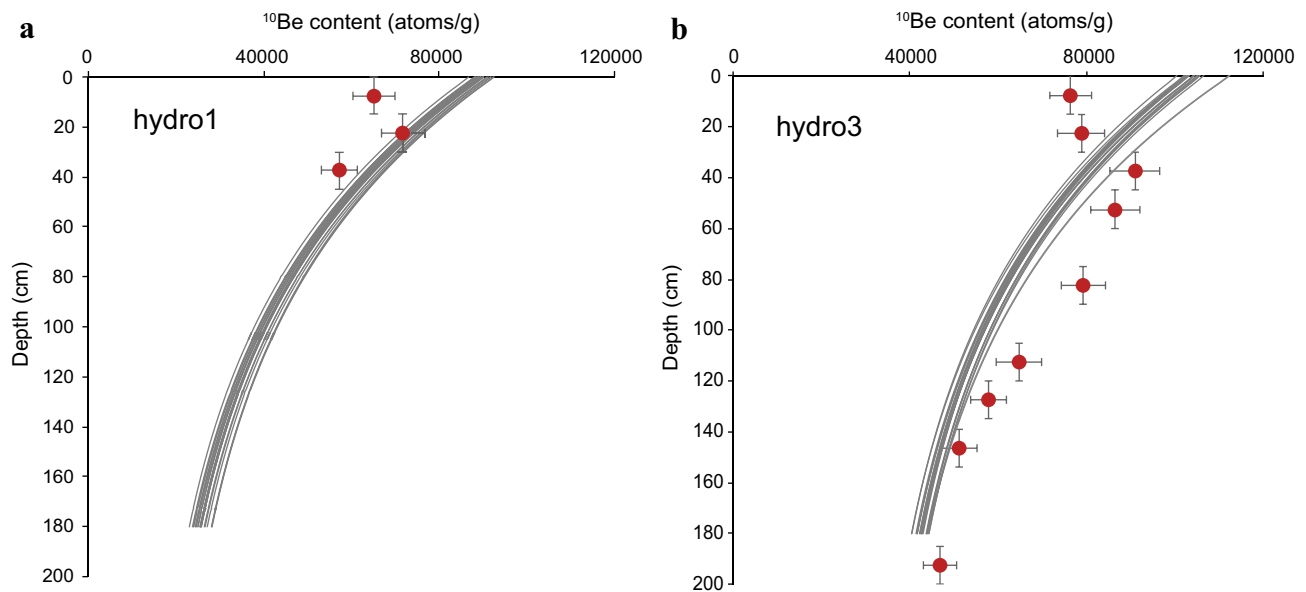


**Fig. 5** In situ  $^{10}\text{Be}$  distribution along the profiles and modelled trend using Eq. 9. Inherited  $^{10}\text{Be}$  and erosion rates were iteratively obtained by minimising the difference between measured and modelled values. **a** Hydro1 and **b** Hydro3

The soil redistribution rates derived from both meteoric and in situ  $^{10}\text{Be}$  are reported in Table 3.

The erosion rates calculated for the site Hydro1 (crest position) are always higher than those of the sites Hydro3 and Hydro4c (backslope and footslope position) independent from the method used, except when using the depth function model (Hidy et al. 2010). When using meteoric  $^{10}\text{Be}$ , the approach of Lal (2001) does not produce a meaningful sequence. When using in situ  $^{10}\text{Be}$ , the calculated soil erosion rates were usually lower. Independent of the type of nuclide used, erosion rates were much lower at the backslope site (i.e. Hydro4c) than at the other sites.

Moreover, we made an independent estimate of soil erosion using a similar methodology as in van der Meij et al. (2017) (Fig. 6). We calculated the current soil thickness using linear regression of depth to C horizon using the logarithm of flow accumulation ( $R^2 = 0.62$ ) with 29 soil observations of the study site. We then derived the soil loss by subtracting the current soil depth from the

mean depth of undisturbed soils (i.e. soils affected by neither erosion nor deposition; 108 cm). The results show the most soil loss at the crest positions (Fig. 6). Soil loss decreases towards the centre of the catchment.

## 5 Discussion

### 5.1 Periods of stability and erosion

The Melzower Forst has a complex history of varying land use and land cover, with stable periods with progressive pedogenesis and unstable periods with regressive pedogenesis in the form of soil erosion. The  $^{14}\text{C}$  dating helped us identify two of these periods.

The oldest  $^{14}\text{C}$  dating of the  $\text{H}_2\text{O}_2$ -resistant fractions indicates a start of carbon uptake and progressive pedogenesis around 17 to 16 kyr BP. This date neatly follows the deglaciation of the area around 19 ka BP (Lüthgens et al. 2011; Hughes et al. 2016; Stroeven et al. 2016).

**Table 3** Long-term soil redistribution rates. Positive values indicate soil erosion/loss

Site	Meteoric $^{10}\text{Be}$		In situ $^{10}\text{Be}$	
	Model used			
	Lal (2001)	Zollinger et al. (2017)	Depth function (Hidy et al. 2010)	Cronus (Balco et al., 2008)
	$\text{t ha}^{-1} \text{ year}^{-1}$	$\text{t ha}^{-1} \text{ year}^{-1}$	$\text{t ha}^{-1} \text{ year}^{-1}$	$\text{t ha}^{-1} \text{ year}^{-1}$
Hydro1	1.62	3.92	0.11	1.20
Hydro3	2.99	0.47	0.19	0.77
Hydro4c	2.83	-3.88	-	0.81

**Table 4** Relationship between physical/chemical properties and meteoric and in situ  $^{10}\text{Be}$ . Numbers reported refer to  $R^2$  values

	Clay (%)	pH (CaCl <sub>2</sub> )	Fe <sub>ox</sub> (g kg <sup>-1</sup> )	Fe <sub>dith</sub> (g kg <sup>-1</sup> )	Al <sub>ox</sub> (g kg <sup>-1</sup> )	Mn <sub>dith</sub> (mg kg <sup>-1</sup> )
met $^{10}\text{Be}$	n.s. †	0.67***§	0.35**†	0.26*†	n.s. †	0.37**†
In situ $^{10}\text{Be}$	-	0.60***§	0.26***§	0.26*†	0.27*§	0.20*†

n.s. not significant

\*  $p$ -value < 0.05; \*\*  $p$ -value < 0.01; \*\*\*  $p$ -value < 0.001

† Linear regression

§ Polynomial regression

This stable phase ended around 7 ka BP, as the  $^{14}\text{C}$  datings from the POM fractions indicate (Table 5). The fAh horizons were all buried about 4.6 to 6.8 ka cal BP. Around this time, the first settlements and agricultural activities started in the region, triggering a regressive phase of soil erosion by deforestation and primitive land management (Schatz 1999; Jahns 2000, 2001; Kulczycka-Leciejewiczowa and Wetzel 2002; Kappler et al. 2018; van der Meij et al. 2019). Kappler et al. (2018) mention that in spite of numerous Neolithic settlements in the study area, no correlative colluvial sediments were detected so far. They attributed first that human-induced soil erosion is attributed to the Late Bronze Age, i.e. c. 4000 years ago. With our  $^{14}\text{C}$  data, we can show that this human-induced erosion most likely started earlier than previously thought and that it better matches with the start of the first settlements in that region. The Melzower Forst was probably also affected by these agricultural activities, because deforestation and land management are the main causes of soil disturbance and erosion in such small catchments. This fits well to records of many sedimentary archives globally, where an increase in erosion rates is often observed 6 to 7 ka BP (Owens 2020). Deforestation and fires can accelerate soil erosion by water distinctly but

cannot explain highest erosion at crest position (according to profile truncation). The observed soil patterns, with most erosion on the convex crests and deposition at the footslopes (Fig. 6), are generally caused by tillage erosion (De Alba et al. 2004; Wilken et al. 2020). The spread in the  $^{14}\text{C}$  ages over such small differences in the depression can indicate a gradual infilling of the colluvium. The same was observed at CarboZALF, where the ages of colluvium can vary hundreds to thousands of years of a distance of tens of metres (van der Meij et al. 2019). Charcoal particles and other burnt organic remnants to testify the human presence and deforestation were not found in any of the buried horizons. Nonetheless, we can hypothesise that a change of land use in the Neolithic (4776–2595 BC) triggered a regressive period in the soil development of the area.

The current stable phase started at least 250 years ago, according to the historical maps. With reforestation of the catchment, the soil-stabilised and progressive pedogenic processes, such as clay translocation, could start again. This especially holds true for Hydro 4c, where distinct E and Bt horizons developed in the colluvial deposits.

With the use of  $^{14}\text{C}$  dating and historical maps, we could identify these three periods of soil and landscape

**Table 5** Analysed soil material and related results of radiocarbon dating

Site/sample	UZH-/ETHZ-code	Material	Depth (cm)	Treatment	C14 age (BP)	$\pm 1\sigma$	cal age (calBP)	
							1 $\sigma$	2 $\sigma$
Hydro4c fAh	UZ-6516/ETH-96758	Soil	180–210	POM	5965	27	6845–6745	6888–6731
Hydro5 fAh	UZ-6518/ETH-96760	Soil	185–213	POM	5128	26	5925–5767	5981–5753
LHS6 fAh	UZ-6515/ETH-96757	Soil	85–108	POM	4741	26	5576–5335	5581–5329
LHS18 fAh	UZ-6517/ETH-96759	Soil	180–210	POM	4067	25	4607–4448	4795–4438
LHS20 fAh	UZ-6519/ETH-96761	Soil	170–219	POM	5609	27	6405–6317	6445–6307
Hydro4c fAh	UZ-6834/ETH-106293.1.1	Soil	180–210	H <sub>2</sub> O <sub>2</sub>	13,895	454	17,560 – 16,161	18,177 – 15,695
Hydro5 fAh	UZ-6836/ETH-106295.1.1	Soil	185–213	H <sub>2</sub> O <sub>2</sub>	9567	270	11,240 – 10,507	11,808 – 10,225
LHS6 fAh	UZ-6833/ETH-106292.1.1	Soil	85–108	H <sub>2</sub> O <sub>2</sub>	8440	254	9696 – 9025	10,180 – 8774
LHS18 fAh	UZ-6835/ETH-106294.1.1	Soil	180–210	H <sub>2</sub> O <sub>2</sub>	9762	283	11,688 – 10,708	12,431 – 10,300
LHS20 fAh	UZ-6837/ETH-106296.1.1	Soil	170–219	H <sub>2</sub> O <sub>2</sub>	9551	348	11,308 – 10,291	12,098 – 9999

POM particulate organic matter (potentially the youngest fraction), H<sub>2</sub>O<sub>2</sub> hydrogen peroxide (H<sub>2</sub>O<sub>2</sub>)-resistant organic matter (potentially the oldest fraction)

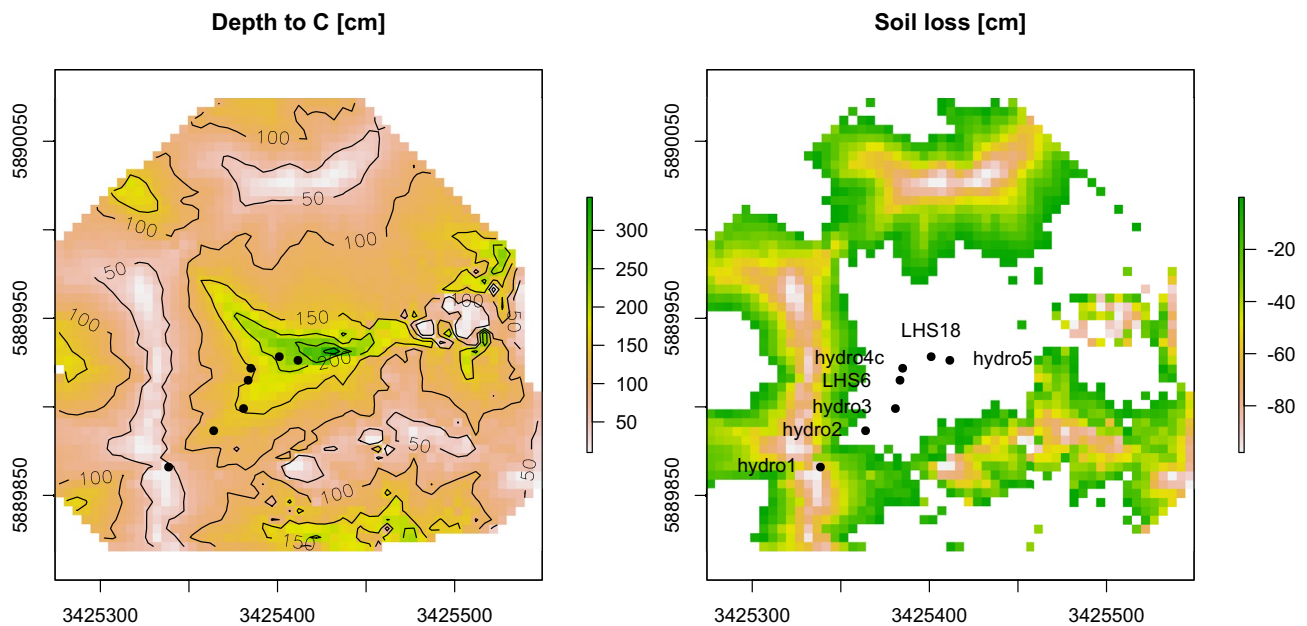


**Fig. 6** Interpolation of the depth to parent material (C horizon; m) and estimation of erosion (soil loss; m)

development in the Melzower Forst. Our findings correlate well with reconstructions of historical land use in the Uckermark region (Jahns 2000; Kappler et al. 2018; van der Meij et al. 2019). Since the beginning of agricultural activities, increased erosion events distinctly affected soils and their characteristics giving rise to a landscape with truncated soil profiles and colluviums. However, there might be more periods that we have not yet identified in the deposits at Melzower Forst, such as periods of abandonment and peaks in settlements of the Bronze Age or the Migration Period (Jahns 2000; Schultz 2009). Additional datings of carbon and sediments throughout the colluvial soil profiles will increase the temporal resolution of the land use reconstruction and can shed light on different periods of landscape stability and instability.

## 5.2 Beryllium-10 ( $^{10}\text{Be}$ ) along the soil profile

The depth trends of meteoric  $^{10}\text{Be}$  in the three profiles are classified in literature as a ‘bulge’ type. In these soils, the peak of the meteoric  $^{10}\text{Be}$  content can be found in a clay-rich B-horizon layer. Graly et al. (2010) showed in their review that this kind of shape is typical for older and slowly eroding soils. The ‘bulge’-type profile of the investigated soils seems rather due to clay translocation than by age and/or slow erosion (Pavich et al. 1984; Egli et al. 2010). Schaller et al. (2018) investigated the contribution of climate and vegetation cover on hillslope denudation in Chile using in situ  $^{10}\text{Be}$  and found ‘bulge’  $^{10}\text{Be}$  depth profiles. In that particular case

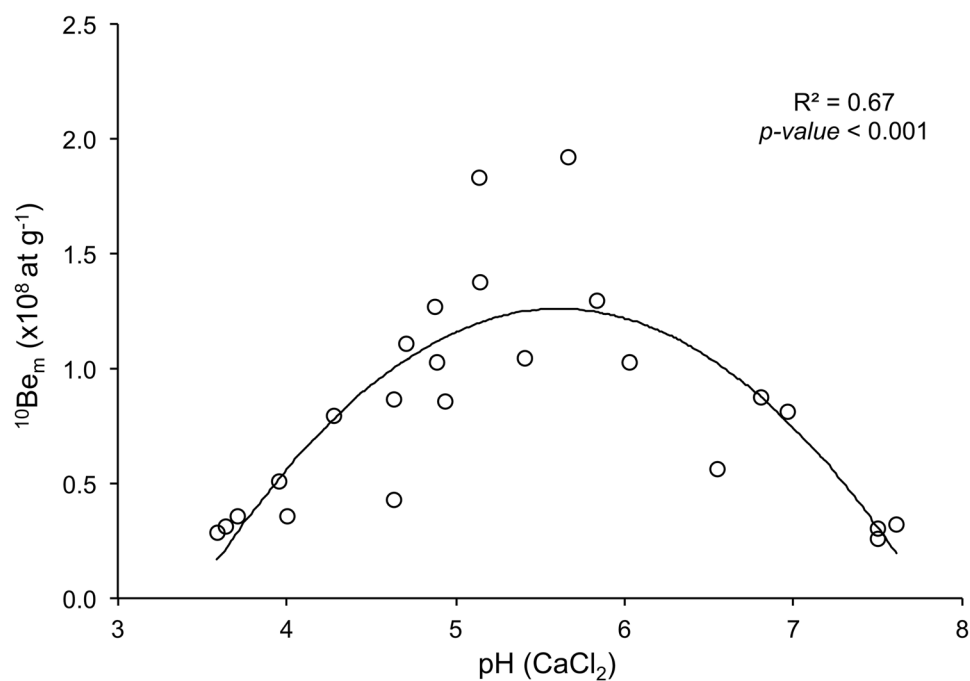
study, the ‘bulge’ shape was attributed to natural soil mixing (e.g. bioturbation).

We compared the  $^{10}\text{Be}$  depth profiles of the present study to  $^{10}\text{Be}$  depth profiles from an agricultural landscape (at the CarboZALF research station; see Calitri et al. 2019) in the same research area (Fig. 4; Table 1). Although the quantities of  $^{10}\text{Be}$  at Melzower Forst are generally higher than those of CarboZALF, the trends of  $^{10}\text{Be}$  along the soil profiles match quite well with each other.

For the erosional site Hydro 1 (Nudiargic Luvisol), the current soil thickness of 30 cm is caused by erosion in the strongly regressive phase that started about 7 ka BP. The soil horizonation of Hydro 1 matches that of profile LP12N at CarboZALF, although the thickness of the Bt is much lower at Hydro 1. Profile morphology corresponds to similar  $^{10}\text{Be}$  depth functions in both profiles.

The profile of Hydro3 (Endostagnic Albic Retisol) in a backslope position shows a complete soil profile (Table 2) and resembles LP4 at CarboZALF. Based on the horizonation and the typical bulge shape of the meteoric  $^{10}\text{Be}$ , erosion of this profile can be assumed minimal. However, in situ  $^{10}\text{Be}$  does not show an increasing content to the soil surface as would be expected from non-eroding soils (Schaller et al. 2018). Instead, the in situ  $^{10}\text{Be}$  content is lower in the topsoil (< 30 cm) compared to horizons just below. We can explain this depth trend by viewing the topsoil of this backslope position as a transport zone, in which erosion and deposition is balanced. The soil profile Hydro4c (Katostagnic Albic Retisol) has developed at a depositional position. In order

**Fig. 7** Relationship between pH and the meteoric (m)  $^{10}\text{Be}$  content in the fine earth fraction



for the sediments to reach the depression, they have to be transported along the slope. The  $^{10}\text{Be}$  content of the transported material decreases, because subsoil material, having a lower  $^{10}\text{Be}$  content, has been exposed at the surface of soils at a higher position along the catena. In consequence, the transported material deposited at Hydro4c represents a mixture of differently eroded (top-)soils from the catchment.

The depositional nature of Hydro4c is supported by the presence of a buried topsoil (fAh), just as profile VAMOS at CarboZALF. The meteoric  $^{10}\text{Be}$  profiles show a similar trend, with an increasing  $^{10}\text{Be}$  content up to the fAh horizon. The in situ  $^{10}\text{Be}$  profiles slightly differ, with a constant  $^{10}\text{Be}$  content at Hydro4c throughout the profile and a small bulge-shape in the  $^{10}\text{Be}$  content at VAMOS.

Although the current land use of Melzower Forst and CarboZALF differ, their  $^{10}\text{Be}$  profiles still match fairly well.

### 5.3 Correlation of $^{10}\text{Be}$ with soil physical and chemical properties

The depth distribution of meteoric  $^{10}\text{Be}$  is controlled by a wide range of factors. In Luvisols and Podzols, meteoric  $^{10}\text{Be}$  may be transported by lessivation and podzolization processes (Pavich et al. 1984; Egli et al. 2010). Despite the documented clay translocation in the region (Sommer et al. 2008; Calitri et al. 2019), which was also observed in the present study (Fig. 3), the correlation with meteoric  $^{10}\text{Be}$  is not significant.

In tropical Oxisols, the meteoric  $^{10}\text{Be}$  is primarily in the oxyhydroxide fraction, which allows more transport to depth

than simple clay translocation (Barg et al. 1997). Indeed, we found a positive correlation with the oxalate-extractable Fe (weakly or non-crystalline forms;  $\text{Fe}_{\text{ox}}$ ), the dithionite-extractable Fe ( $\text{Fe}_{\text{dith}}$ ) and dithionite-extractable  $\text{Mn}_{\text{dith}}$  (Table 4). Meteoric  $^{10}\text{Be}$  can be incorporated as a cation in oxyhydroxide complexes (Barg et al. 1997; Takahashi et al. 1999). Therefore, the distribution pattern of meteoric  $^{10}\text{Be}$  is governed to a certain extent by Fe–Mn oxyhydroxides.

Wyshnytzky et al. (2015) and Campforts et al. (2016) identified pH as one of the key variables controlling meteoric  $^{10}\text{Be}$  sorption reactions. In contrast, Graly et al. (2010) did not find a statistically significant effect of soil pH on meteoric  $^{10}\text{Be}$ . According to Boschi and Willenbring (2021), the cation exchange capacity and the inverse abundance of quartz best predict Be sorption. Similarly, Chen et al. (2020) argue that grain size, mineralogy, pH and cation exchange capacity control the  $^{10}\text{Be}$  contents in soils. The cation exchange capacity is influenced by soil acidity. In our investigated soils, pH seems to exert an influence on meteoric  $^{10}\text{Be}$  (Fig. 7); the processes or factors that lead to this non-linear pattern, however, seem diverse. In the pH range 3.5–5.5, meteoric  $^{10}\text{Be}$  decreases with decreasing pH. This effect points to chemical leaching (transport in dissolved forms) and translocation with clay particles. As already pointed out by Heyn (1989) and Keilen et al. (1977), a decreasing pH increases the solubility of Be. The E-horizons often have a pH-value < 5 indicating a leaching of soluble  $^{10}\text{Be}$  and co-translocation with clays. An active clay migration at Hydro4c in the top 40 cm is strongly limited to inexistent owing to a too low pH. Here, solute

transport seems to dominate while at the sites Hydro1 and Hydro4 predominantly clay migration or a combination with solute transport is the determining process. In the pH range  $> 6$  to  $7.7$ , the contents of meteoric  $^{10}\text{Be}$  decrease with increasing pH. This is due to the fact that high pH values are encountered in the subsoil or parent material where only a small amount of  $^{10}\text{Be}$  accumulated (Table 5).

#### 5.4 Soil redistribution rates

The calculated soil redistribution rates vary substantially, depending on the type of  $^{10}\text{Be}$  and the model that are used to calculate the rates. The calculated erosion rates vary from  $0.1$  to  $3.9$  t/ha/year (Table 3); in some situations, accumulation was determined. The erosion rates correspond to a soil loss of  $0.1$  to  $3.1$  m over the entire Holocene. These rates seem too high for (pre-)historic agricultural erosion and would require unrealistic high soil development rates. The measured accumulation rates using meteoric  $^{10}\text{Be}$  for the last  $6.8$  kyr (Hydro 4c) give a deposition of about  $1.7$  m which corresponds quite exactly to the soil layer measured above the buried horizon at this site.

We estimated the spatial pattern of soil loss in Fig. 6. If we divide the estimated soil loss by the surface age of the investigated site of  $19$  ka, we obtain an estimate of the spatial variation in long-term soil erosion. The average erosion rate for the entire catchment is  $0.3 \pm 0.2$  t ha $^{-1}$  year $^{-1}$ . For the Hydro1 site, the long-term erosion rates range from  $0.6$  to  $0.8$  t ha $^{-1}$  year $^{-1}$ . These rates are in the same order of magnitude as the soil redistribution rates calculated using in situ  $^{10}\text{Be}$ . Based on the estimated soil loss, there was no erosion at the Hydro3 and Hydro4c sites, because their interpolated soil thickness exceeded the reference thickness. The distribution pattern of these calculations match with the results obtained from  $^{10}\text{Be}$  (calculate version using the approach of Zollinger et al. 2017). The absolute values of erosion however differ (with higher values when using  $^{10}\text{Be}$  compared to this modelling approach).

The calculated rates are higher than long-term, large-scale erosion rates calculated for middle European river catchments ( $0.3$ – $1.5$  t/ha/year, Schaller et al. 2001). However, the catchment of the Melzower Forst is much smaller than those of the European rivers studied by Schaller et al. (2001), which would indicate severe erosion and deposition in the Melzower Forst. Also, the calculated erosion rates using in situ  $^{10}\text{Be}$  are higher than those at CarboZALF ( $0.03$ – $1.61$  t/ha/year, Calitri et al. 2019). This is surprising, because the CarboZALF site has been intensively used in the last centuries, especially since the Second World War, contrary to the Melzower Forst that was forested in that period. This period after the Second World War is generally considered to be the

most erosive, due to intensification of agriculture and increase of machine power (Frielinghaus and Vahrson 1998; Sommer et al. 2008).

Other difficulties may arise in the estimation of erosion rates using in situ  $^{10}\text{Be}$  if a model (e.g. CRONUS) considers only the topsoil. The approach according to Zollinger et al. (2017) and Hidy et al. (2010) have problems in solving bulge-shaped  $^{10}\text{Be}$  distribution profiles that are due to clay translocation, bioturbation or other processes. An additional error source might be the difficulty in precisely estimating the input rate of meteoric  $^{10}\text{Be}$ . The meteoric  $^{10}\text{Be}$  flux on Earth's surface is the most critical parameter in estimating soil erosion rates (Chen et al. 2020; Derakhshan-Babaei et al. 2020). Therefore, the calculation of soil erosion or denudation rates using  $^{10}\text{Be}$  may be prone to errors depending on the environmental settings. The calculated erosion rates at Melzower Forst using  $^{10}\text{Be}$  are higher than expected. An explanation for this can be found in the complex erosion and land use history of Melzower Forst and the limitations of the applied Beryllium-erosion models to account for different phases of erosion and stability. The soil deposition rates, however, seem to match the conditions.

At Melzower Forst, periods with erosion and deposition alternated with more stable conditions. When calculating erosion rates using in situ or meteoric  $^{10}\text{Be}$ , an average value over the entire soil development period (i.e. since the last deglaciation and Holocene) is obtained. This includes therefore also stable periods, where little or no erosion has occurred. Consequently, the erosion rates are underestimated in periods (like  $7$  kyr BP– $250$  years ago) having instable and regressive conditions and overestimated for stable periods having progressive conditions for soil formation.

Soil removal from eroding positions, transport over the hillslope and deposition in the depression affected the Beryllium profiles differently at different hillslope positions. The current Be profiles are a product of alternating periods of stability and erosion and landscape position. To disentangle the Be-profiles and reconstruct the erosion history, the used model approaches for  $^{10}\text{Be}$  have some difficulties. Numerical process-based models may help in explaining the complex soil mass redistribution (e.g. Campforts et al. 2016).

## 6 Conclusions

The application of meteoric and in situ  $^{10}\text{Be}$  and  $^{14}\text{C}$  dating along a soil catena in a small forested catchment revealed progressive and regressive phases of soil evolution. Meteoric and in situ  $^{10}\text{Be}$  exhibited sometimes depth profiles with a 'bulge' shape. Clay translocation can explain in part the profile distribution of meteoric  $^{10}\text{Be}$ , but not only. The depth trend of in situ  $^{10}\text{Be}$  along the profiles at the mid-slope position is more or less according to the expectances.

In addition, in situ  $^{10}\text{Be}$  revealed the different layers and enabled a differentiation between buried horizons, deposited material, biologically reworked and redistributed material. The footslope soil did not show any depth trend and exhibits strongly depositional conditions. The crest position had the lowest  $^{10}\text{Be}$  content for both, meteoric and in situ  $^{10}\text{Be}$ . Although the Melzower forest is protected and has been a forest since least 250 years,  $^{10}\text{Be}$  clearly indicates major soil mass redistribution along the investigated catena. The calculation of soil deposition rates using meteoric  $^{10}\text{Be}$  gave realistic values. The determination of meaningful erosion rates was, however, difficult — independent of the type of  $^{10}\text{Be}$  and related model for rate calculations. Furthermore, we applied an independent spatial modelling approach where the current soil thickness was related to flow accumulation. Knowing soil depth distribution and their age, the erosion patterns and rates could be calculated. Using this procedure, a quality check with the  $^{10}\text{Be}$  results was enabled. The soil redistribution rates (over the entire period of soil formation) were similar to those obtained from a nearby area that is used for intense agriculture (CarboZALF area). This means that the effects of the past, long-term soil mass redistribution still overshadow the present-day erosion.

The  $^{14}\text{C}$  ages of buried soil horizons point to strongly regressive soil development phases (with erosion and deposition) that started particularly between about 4.5 and 6.8 kyr BP. Although absolute proofs are lacking, this seems to be due to human impact that started to increasingly affect soil properties at that time. The temporal erosion pattern fits with archaeological finds of first settlement in the region around 7 kyr BP. However, stronger soil erosional signals were so far dated back to about max 5 kyr BP. We show now that strong erosional processes already occurred earlier and seem to coincide with the onset of these settlements.

**Supplementary information** The online version contains supplementary material available at <https://doi.org/10.1007/s11368-021-03041-7>.

**Funding** Open Access funding provided by Universität Zürich. This research was supported by a cooperation contract (CORRELATE; F-75113–07-01) between the University of Zurich and the ZALF.

**Open Access** This article is licensed under a Creative Commons Attribution 4.0 International License, which permits use, sharing, adaptation, distribution and reproduction in any medium or format, as long as you give appropriate credit to the original author(s) and the source, provide a link to the Creative Commons licence, and indicate if changes were made. The images or other third party material in this article are included in the article's Creative Commons licence, unless indicated otherwise in a credit line to the material. If material is not included in the article's Creative Commons licence and your intended use is not permitted by statutory regulation or exceeds the permitted use, you will need to obtain permission directly from the copyright holder. To view a copy of this licence, visit <http://creativecommons.org/licenses/by/4.0/>.

## References

- Bacon AR, Richter D, deB., Bierman PR, Rood DH (2012) Coupling meteoric  $^{10}\text{Be}$  with pedogenic losses of  $^9\text{Be}$  to improve soil residence time estimates on an ancient North American interfluvium. *Geology* 40:847–850. <https://doi.org/10.1130/G33449.1>
- Balco G, Stone JO, Lifton NA, Dunai TJ (2008) A complete and easily accessible means of calculating surface exposure ages or erosion rates from  $^{10}\text{Be}$  and  $^{26}\text{Al}$  measurements. *Prospects New Front Earth Environ Sci* 3:174–195. <https://doi.org/10.1016/j.jquageo.2007.12.001>
- Banner JL (2004) Radiogenic isotopes: systematics and applications to earth surface processes and chemical stratigraphy. *Earth-Sci Rev* 65:141–194. [https://doi.org/10.1016/S0012-8252\(03\)00086-2](https://doi.org/10.1016/S0012-8252(03)00086-2)
- Barg E, Lal D, Pavich MJ, Caffee MW, Southon JR (1997) Beryllium geochemistry in soils: evaluation of  $^{10}\text{Be}/^9\text{Be}$  ratios in authigenic minerals as a basis for age models. *Chem Geol* 140:237–258. [https://doi.org/10.1016/S0009-2541\(97\)00051-X](https://doi.org/10.1016/S0009-2541(97)00051-X)
- Birkeland PW, Shroba RR, Burns SF, Price AB, Tonkin PJ (2003) Integrating soils and geomorphology in mountains - an example from the Front Range of Colorado. *Geomorphology* 55:329–344. [https://doi.org/10.1016/S0169-555X\(03\)00148-X](https://doi.org/10.1016/S0169-555X(03)00148-X)
- Boschi V, Willenbring JK (2021) Chemical and physical drivers of beryllium retention in two soil endmembers. *Sci Total Environ* 754:141591. <https://doi.org/10.1016/j.scitotenv.2020.141591>
- Brevik EC, Hartemink AE (2010) Early soil knowledge and the birth and development of soil science. *CATENA* 83:23–33. <https://doi.org/10.1016/j.catena.2010.06.011>
- Bronk Ramsey C (2001) Development of the radiocarbon calibration program. *Radiocarbon* 43:355–363. <https://doi.org/10.1017/S0033822200038212>
- Bronk Ramsey C (2009) Bayesian analysis of radiocarbon dates. *Radiocarbon* 51:337–360. <https://doi.org/10.1017/S0033822200033865>
- Calitri F, Sommer M, van der Meij MW, Egli M (2020) Soil erosion along a transect in a forested catchment: Recent or ancient processes? *CATENA* 194:104683. <https://doi.org/10.1016/j.catena.2020.104683>
- Calitri F, Sommer M, Norton K, Temme A, Brandová D, Portes R, Christl M, Ketterer ME, Egli M (2019) Tracing the temporal evolution of soil redistribution rates in an agricultural landscape using  $^{239+240}\text{Pu}$  and  $^{10}\text{Be}$ . *Earth Surf Process Landf* 44:1783–1798. <https://doi.org/10.1002/esp.4612>
- Campforts B, Vanacker V, Vanderborght J, Baken S, Smolders E, Govers G (2016) Simulating the mobility of meteoric  $^{10}\text{Be}$  in the landscape through a coupled soil-hillslope model (Be2D). *Earth Planet Sci Lett* 439:143–157. <https://doi.org/10.1016/j.epsl.2016.01.017>
- Chen P, Yi P, Czymzik M, Aldahan A, Ljung K, Yu Z, Hou X, Zheng M, Chen X, Possnert G (2020) Relationship between precipitation and  $^{10}\text{Be}$  and impacts on soil dynamics. *CATENA* 195:104748. <https://doi.org/10.1016/j.catena.2020.104748>
- Christl M, Vockenhuber C, Kubik PW, Wacker L, Lachner J, Alfimov V, Synal H-A (2013) The ETH Zurich AMS facilities: Performance parameters and reference materials. *Nucl Instrum Methods Phys Res Sect B Beam Interact Mater* at 294:29–38. <https://doi.org/10.1016/j.nimb.2012.03.004>
- De Alba S, Lindstrom M, Schumacher TE, Malo DD (2004) Soil landscape evolution due to soil redistribution by tillage: a new conceptual model of soil catena evolution in agricultural landscapes. *CATENA* 58:77–100. <https://doi.org/10.1016/j.catena.2003.12.004>
- Derakhshan-Babaei F, Nosrati K, Tikhomirov D, Christl M, Sadough H, Egli M (2020) Relating the spatial variability of chemical weathering and erosion to geological and topographical zones. *Geomorphology* 363:107235. <https://doi.org/10.1016/j.geomorph.2020.107235>



- Dosseto A, Schaller M (2016) The erosion response to Quaternary climate change quantified using uranium isotopes and in situ-produced cosmogenic nuclides. *Earth-Sci Rev* 155:60–81. <https://doi.org/10.1016/j.earscirev.2016.01.015>
- Egli M, Brandová D, Böhlert R, Favilli F, Kubik PW (2010) <sup>10</sup>Be inventories in Alpine soils and their potential for dating land surfaces. *Geomorphology* 119:62–73. <https://doi.org/10.1016/j.geomorph.2010.02.019>
- Eusterhues K, Rumpel C, Kögel-Knabner I (2005) Stabilization of soil organic matter isolated via oxidative degradation. *Org Geochem* 36:1567–1575. <https://doi.org/10.1016/j.orggeochem.2005.06.010>
- FAO (Food and Agriculture Organization of the United Nations) (2006) Guidelines for soil description. FAO, Rome
- Favilli F, Egli M, Brandová D, Ivy-Ochs S, Kubik PW, Maisch M, Cherubini P, Haerberli W (2009) Combination of numerical dating techniques using <sup>10</sup>Be in rock boulders and <sup>14</sup>C of resilient soil organic matter for reconstructing the chronology of glacial and periglacial processes in a high Alpine catchment during the Late Pleistocene and Early Holocene. *Radiocarbon* 51:537–552. <https://doi.org/10.1017/S0033822200055910>
- Favilli F, Egli M, Cherubini P, Sartori G, Haerberli W, Delbos E (2008) Comparison of different methods of obtaining a resilient organic matter fraction in Alpine soils. *Model Pedogenesis* 145:355–369. <https://doi.org/10.1016/j.geoderma.2008.04.002>
- Frielinghaus M, Vahrson W-G (1998) Soil translocation by water erosion from agricultural cropland into wet depressions (morainic kettle holes). *Soil Tillage Res* 46:23–30. [https://doi.org/10.1016/S0167-1987\(98\)80104-9](https://doi.org/10.1016/S0167-1987(98)80104-9)
- Graly JA, Bierman PR, Reusser LJ, Pavich MJ (2010) Meteoric <sup>10</sup>Be in soil profiles - a global meta-analysis. *Geochim Cosmochim Acta* 74:6814–6829. <https://doi.org/10.1016/j.gca.2010.08.036>
- Granger DE, Riebe CS (2007) 5.19 - cosmogenic nuclides in weathering and erosion. In: Holland HD, Turekian KK (eds) *Treatise on Geochemistry*. Pergamon, Oxford, pp 1–43
- Granger DE, Riebe CS (2014) 7.12 - cosmogenic nuclides in weathering and erosion. In: Holland HD, Turekian KK (eds) *Treatise on geochemistry (Second Edition)*, 2nd edn. Elsevier, Oxford, pp 401–436
- Heimsath AM (2006) Eroding the land: steady-state and stochastic rates and processes through a cosmogenic lens. In: Alonso-Zarza AM, Tanner LH (eds) *In Situ-Produced Cosmogenic Nuclides and Quantification of Geological Processes*. *Geol Soc Am* pp 111–129
- Heimsath AM, Dietrich WE, Nishiizumi K, Finkel RC (1997) The soil production function and landscape equilibrium. *Nature* 388:358–361. <https://doi.org/10.1038/41056>
- Helfrich M, Flessa H, Mikutta R, Dreves A, Ludwig B (2007) Comparison of chemical fractionation methods for isolating stable soil organic carbon pools. *Eur J Soil Sci* 58:1316–1329. <https://doi.org/10.1111/j.1365-2389.2007.00926.x>
- Hey B (1989) Elementflüsse und Elementbilanzen in Waldökosystemen der Bärhalde — Südschwarzwald. *Freiburger Bodenkundliche Abhandlungen*, Heft 23, Institut für Bodenkunde und Waldernährungslehre der Albert-Ludwigs-Universität, Freiburg, Germany
- Hidy AJ, Gosse JC, Pederson JL, Mattern JP, Finkel RC (2010) A geologically constrained Monte Carlo approach to modeling exposure ages from profiles of cosmogenic nuclides: an example from Lees Ferry Arizona. *Geochem Geophys Geosystems* 11 <https://doi.org/10.1029/2010GC003084>
- Hughes ALC, Gyllencreutz R, Lohne ØS, Mangerud J, Svendsen JI (2016) The last Eurasian ice sheets – a chronological database and time-slice reconstruction, DATED-1. *Boreas* 45:1–45. <https://doi.org/10.1111/bor.12142>
- IUSS Working Group WRB (2015) World Reference Base for Soil Resources 2014, update 2015 International soil classification system for naming soils and creating legends for soil maps. FAO, Rome
- Ivy-Ochs S, Kober F (2008) Surface exposure dating with cosmogenic nuclides. *EG Quat Sci J* 57:179–209. <https://doi.org/10.3285/eg.57.1-2.7>
- Jahns S (2000) Late-glacial and Holocene woodland dynamics and land-use history of the Lower Oder valley, north-eastern Germany, based on two, AMS <sup>14</sup>C-dated, pollen profiles. *Veg Hist Archaeobotany* 9:111–123. <https://doi.org/10.1007/BF01300061>
- Jahns S (2001) On the Late Pleistocene and Holocene history of vegetation and human impact in the Ucker valley, north-eastern Germany. *Veg Hist Archaeobotany* 10:97–104. <https://doi.org/10.1007/PL00006924>
- Jenny H (1984) The soil resource. *Origin and Behavior Vegetatio* 57:102–102. <https://doi.org/10.1007/BF00047304>
- Jungers MC, Bierman PR, Matmon A, Nichols K, Larsen J, Finkel R (2009) Tracing hillslope sediment production and transport with in situ and meteoric <sup>10</sup>Be. *J Geophys Res Earth Surf* 114:F04020. <https://doi.org/10.1029/2008JF001086>
- Kappler C, Kaiser K, Tanski P, Klos F, Fülling A, Mrotzek A, Sommer M, Bens O (2018) Stratigraphy and age of colluvial deposits indicating Late Holocene soil erosion in northeastern Germany. *CATENA* 170:224–245. <https://doi.org/10.1016/j.catena.2018.06.010>
- Keilen K, Stahr K, Goltz H, v. d, Zöttl HW, (1977) Zur pedochemie des berylliums — untersuchungen einer bodengesellschaft im gebiet des bärhaldegranits (südschwarzwald). *Geoderma* 17:315–329. [https://doi.org/10.1016/0016-7061\(77\)90092-1](https://doi.org/10.1016/0016-7061(77)90092-1)
- Kögel-Knabner I, Guggenberger G, Kleber M, Kandeler E, Kalbitz K, Scheu S, Eusterhues K, Leinweber P (2008) Organo-mineral associations in temperate soils: Integrating biology, mineralogy, and organic matter chemistry. *J Plant Nutr Soil Sci* 171:61–82. <https://doi.org/10.1002/jpln.200700048>
- Kopp D, Schwanecke W (1994) *Standörtlich-naturräumliche Grundlagen ökologischer Forstwirtschaft*. Dtsch Landwirtschaftsverlag Berl GmbH
- Koszinski S, Gerke HH, Hierold W, Sommer M (2013) Geophysical-based nodelling of a kettle hole catchment of the morainic soil landscape. *Vadose Zone J* 12:1–18. <https://doi.org/10.2136/vzj2013.02.0044>
- Kulczycka-Leciejewiczowa A, Wetzel G (2002) Neolithikum im Odergebiet, [w:] E. Gringmuth-Dallmer, L. Leciejewicz (Eds.), *Forschungen zu Mensch und Umwelt im Odergebiet in frühgeschichtlicher Zeit*. pp. 257–270
- Lal D (2001) New nuclear methods for studies of soil dynamics utilizing cosmic ray produced radionuclides. In: Stott, D.E., Mohtar, R.H., Steinhardt, G.C.(Eds.) *Sustaining the global farm*. 10th International Soil Conservation Organization Meeting, Purdue University and USDA-ARS National Soil Erosion Research Laboratory. pp 1044–1052
- Lüthgens C, Böse M, Preusser F (2011) Age of the Pomeranian ice-marginal position in northeastern Germany determined by Optically Stimulated Luminescence (OSL) dating of glaciofluvial sediments. *Boreas* 40:598–615. <https://doi.org/10.1111/j.1502-3885.2011.00211.x>
- Maejima Y, Matsuzaki H, Higashi T (2005) Application of cosmogenic <sup>10</sup>Be to dating soils on the raised coral reef terraces of Kikai Island, southwest Japan. *Geoderma* 126:389–399. <https://doi.org/10.1016/j.geoderma.2004.10.004>
- Masarik J, Beer J (2009) An updated simulation of particle fluxes and cosmogenic nuclide production in the Earth's atmosphere. *J Geophys Res Atmospheres* 114:D11103. <https://doi.org/10.1029/2008JD010557>
- McKean JA, Dietrich WE, Finkel RC, Southon JR, Caffee MW (1993) Quantification of soil production and downslope creep rates from cosmogenic <sup>10</sup>Be accumulations on a hillslope profile. *Geology* 21:343–346. [https://doi.org/10.1130/0091-7613\(1993\)021%3c0343:QOSPAD%3e2.3.CO;2](https://doi.org/10.1130/0091-7613(1993)021%3c0343:QOSPAD%3e2.3.CO;2)

- Minasny B, Finke P, Stockmann U, Vanwalleghem T, McBratney AB (2015) Resolving the integral connection between pedogenesis and landscape evolution. *Earth-Sci Rev* 150:102–120. <https://doi.org/10.1016/J.EARSCIREV.2015.07.004>
- Minasny B, McBratney AB (2006) A conditioned Latin hypercube method for sampling in the presence of ancillary information. *Comput Geosci* 32:1378–1388. <https://doi.org/10.1016/j.cageo.2005.12.009>
- Montgomery DR (2007) Soil erosion and agricultural sustainability. *Proc Natl Acad Sci* 104:13268–13272. <https://doi.org/10.1073/pnas.0611508104>
- Norton KP, von Blanckenburg F, Kubik PW (2010) Cosmogenic nuclide-derived rates of diffusive and episodic erosion in the glacially sculpted upper Rhone Valley, Swiss Alps. *Earth Surf Process Landf* 35:651–662. <https://doi.org/10.1002/esp.1961>
- Owens PN (2020) Soil erosion and sediment dynamics in the Anthropocene: a review of human impacts during a rapid global environmental change. *J Soil Sediment* 20:4115–4143. <https://doi.org/10.1007/s11368-020-02815-9>
- Pavich MJ (1989) Regolith residence time and the concept of surface age of the Piedmont “Peneplain.” *Geomorphology* 2:181–196. [https://doi.org/10.1016/0169-555X\(89\)90011-1](https://doi.org/10.1016/0169-555X(89)90011-1)
- Pavich MJ, Brown L, Klein J, Middleton R (1984)  $^{10}\text{Be}$  accumulation in a soil chronosequence. *Earth Planet Sci Lett* 68:198–204. [https://doi.org/10.1016/0012-821X\(84\)90151-1](https://doi.org/10.1016/0012-821X(84)90151-1)
- Preusser F, Degering D, Fuchs M, Hilgers A, Kadereit A, Klasen N, Krbetschek M, Richter D, Spencer JQG (2008) Luminescence dating: basics, methods and applications. *EG Quat Sci J* 57:95–149. <https://doi.org/10.3285/eg.57.1-2.5>
- Reimer PJ, Austin WEN, Bard E, Bayliss A, Blackwell PG, Bronk Ramsey C, Butzin M, Cheng H, Edwards RL, Friedrich M, Grootes PM, Guilderson TP, Hajdas I, Heaton TJ, Hogg AG, Hughen KA, Kromer B, Manning SW, Muscheler R, Palmer JG, Pearson C, van der Plicht J, Reimer RW, Richards DA, Scott EM, Southon JR, Turney CSM, Wacker L, Adolphi F, Büntgen U, Capano M, Fahrni SM, Fogtmann-Schulz A, Friedrich R, Köhler P, Kudsk S, Miyake F, Olsen J, Reinig F, Sakamoto M, Sookdeo A, Talamo S (2020) The IntCal20 northern hemisphere radiocarbon age calibration curve (0–55 cal kBP). *Radiocarbon* 62:725–757. <https://doi.org/10.1017/RDC.2020.41>
- Rüffer O (2018) Standortsspezifische Entwicklung von Buchenwaldgesellschaften im nordostdeutschen Tiefland, dargestellt am Beispiel des Melzower Buchennaturwaldes. Humboldt-Universität Berlin Germany
- Ryan JG (2002) Trace-element systematics of beryllium in terrestrial materials. *Rev Mineral Geochem* 50:121–145. <https://doi.org/10.2138/rmg.2002.50.3>
- Šamonil P, Daněk P, Adam D, Phillips JD (2017) Breakage or uprooting: how tree death type affects hillslope processes in old-growth temperate forests. *Geomorphology* 299:76–84. <https://doi.org/10.1016/j.geomorph.2017.09.023>
- Schaller M, Ehlers TA, Lang KAH, Schmid M, Fuentes-Espoz JP (2018) Addressing the contribution of climate and vegetation cover on hillslope denudation, Chilean Coastal Cordillera (26°–38°S). *Earth Planet Sci Lett* 489:111–122. <https://doi.org/10.1016/j.epsl.2018.02.026>
- Schaller M, von Blanckenburg F, Hovius N, Kubik PW (2001) Large-scale erosion rates from in situ-produced cosmogenic nuclides in European river sediments. *Earth Planet Sci Lett* 188:441–458. [https://doi.org/10.1016/S0012-821X\(01\)00320-X](https://doi.org/10.1016/S0012-821X(01)00320-X)
- Schatz T (1999) Untersuchungen zur holozänen Landschaftsentwicklung Nordost-Deutschlands. Doctoral thesis
- Schlichting E, Blume HP, Stahr K (1995) *Soils practical* (in German). Blackwell, Berlin
- Schoonejans J, Vanacker V, Opfergelt S, Christl M (2017) Long-term soil erosion derived from in-situ  $^{10}\text{Be}$  and inventories of meteoric  $^{10}\text{Be}$  in deeply weathered soils in southern Brazil. *Chem Geol* 466:380–388. <https://doi.org/10.1016/j.chemgeo.2017.06.025>
- Schulz M (2009) Ur- und Frühgeschichte des Prenzlauer Raumes: von den Anfängen der menschlichen Besiedlung bis zu den Anfängen der Stadt im 13. Jahrhundert. In: Neitmann K, Schich W (eds) *Geschichte der Stadt Prenzlau*. Geiger-Verlag, Horb am Neckar, pp 15–26
- Siame L, Bellier O, Braucher R, Sébrier M, Cushing M, Bourlès D, Hamelin B, Baroux E, de Voogd B, Raisbeck G, Yiou F (2004) Local erosion rates versus active tectonics: cosmic ray exposure modelling in Provence (south-east France). *Earth Planet Sci Lett* 220:345–364. [https://doi.org/10.1016/S0012-821X\(04\)00061-5](https://doi.org/10.1016/S0012-821X(04)00061-5)
- Sommer M, Gerke HH, Deumlich D (2008) Modelling soil landscape genesis — A “time split” approach for hummocky agricultural landscapes. *Model Pedogenesis* 145:480–493. <https://doi.org/10.1016/j.geoderma.2008.01.012>
- Stroeven AP, Hätttestrand C, Kleman J, Heyman J, Fabel D, Fredin O, Goodfellow BW, Harbor JM, Jansen JD, Olsen L, Caffee MW, Fink D, Lundqvist J, Rosqvist GC, Strömberg B, Jansson KN (2016) Deglaciation of Fennoscandia. *Spec Issue PAST Gateway Palaeo-Arct Spat Temporal Gateway* 147:91–121. <https://doi.org/10.1016/j.quascirev.2015.09.016>
- Takahashi Y, Minai Y, Ambe S, Makide Y, Ambe F (1999) Comparison of adsorption behavior of multiple inorganic ions on kaolinite and silica in the presence of humic acid using the multitracer technique. *Geochim Cosmochim Acta* 63:815–836. [https://doi.org/10.1016/S0016-7037\(99\)00065-4](https://doi.org/10.1016/S0016-7037(99)00065-4)
- Troeh FR, Hobbs JA, Donahue RL (1981) Soil and water conservation for productivity and environmental protection. *Soil Sci* 132
- van der Meij WM, Reimann T, Vornehm VK, Temme AJAM, Wallinga J, van Beek R, Sommer M (2019) Reconstructing rates and patterns of colluvial soil redistribution in agrarian (hummocky) landscapes. *Earth Surf Process Landf* 44:2408–2422. <https://doi.org/10.1002/esp.4671>
- van der Meij WM, Temme AJAM, Lin HS, Gerke HH, Sommer M (2018) On the role of hydrologic processes in soil and landscape evolution modeling: concepts, complications and partial solutions. *Earth-Sci Rev* 185:1088–1106. <https://doi.org/10.1016/j.earscirev.2018.09.001>
- van der Meij WM, Temme AJAM, Wallinga J, Hierold W, Sommer M (2017) Topography reconstruction of eroding landscapes – a case study from a hummocky ground moraine (CarboZALF-D). *Geomorphology* 295:758–772. <https://doi.org/10.1016/j.geomorph.2017.08.015>
- van Noordwijk M, Cerri C, Woomer PL, Nugroho K, Bernoux M (1997) Soil carbon dynamics in the humid tropical forest zone. *Geoderma* 79:187–225. [https://doi.org/10.1016/S0016-7061\(97\)00042-6](https://doi.org/10.1016/S0016-7061(97)00042-6)
- Van Oost K, Quine TA, Govers G, De Gryze S, Six J, Harden JW, Ritchie JC, McCarty GW, Heckrath G, Kosmas C, Giraldez JV, da Silva JRM, Merckx R (2007) The impact of agricultural soil erosion on the global carbon cycle. *Science* 318:626–629. <https://doi.org/10.1126/science.1145724>
- Van Oost K, Van Muysen W, Govers G, Deckers J, Quine TA (2005) From water to tillage erosion dominated landform evolution. *Geomorphology* 72:193–203. <https://doi.org/10.1016/j.geomorph.2005.05.010>
- West N, Kirby E, Bierman P, Slingerland R, Ma L, Rood D, Brantley S (2013) Regolith production and transport at the Susquehanna Shale Hills Critical Zone Observatory, part 2: insights from meteoric  $^{10}\text{Be}$ . *J Geophys Res Earth Surf* 118:1877–1896. <https://doi.org/10.1002/jgrf.20121>
- Wilken F, Ketterer M, Koszinski S, Sommer M, Fiener P (2020) Understanding the role of water and tillage erosion from  $^{239+240}\text{Pu}$  tracer measurements using inverse modelling. *SOIL* 6:549–564. <https://doi.org/10.5194/soil-6-549-2020>

- Willenbring JK, von Blanckenburg F (2010) Meteoric cosmogenic Beryllium-10 adsorbed to river sediment and soil: pplications for Earth-surface dynamics. *Earth-Sci Rev* 98:105–122. <https://doi.org/10.1016/j.earscirev.2009.10.008>
- Wyshnytzky CE, Ouimet WB, McCarthy J, Dethier DP, Shroba RR, Bierman PR, Rood DH (2015) Meteoric  $^{10}\text{Be}$ , clay, and extractable iron depth profiles in the Colorado Front Range: implications for understanding soil mixing and erosion. *CATENA* 127:32–45. <https://doi.org/10.1016/j.catena.2014.12.008>
- Zollinger B, Alewell C, Kneisel C, Brandová D, Petrillo M, Plötze M, Christl M, Egli M (2017) Soil formation and weathering in a permafrost environment of the Swiss Alps: a multi-parameter and non-steady-state approach. *Earth Surf Process Landf* 42:814–835. <https://doi.org/10.1002/esp.4040>

**Publisher's Note** Springer Nature remains neutral with regard to jurisdictional claims in published maps and institutional affiliations.